In: beim Graben, P., Zhou, C., Thiel, M. & Kurths, J.(Eds.)
Lectures in Supercomputational Neuroscience:
Dynamics in Complex Brain Networks. Berlin: Springer, 2008.

1

Foundations of Neurophysics

Peter beim Graben[1,2]

[1] School of Psychology and Clinical Language Sciences,
University of Reading, United Kingdom
p.r.beimgraben@reading.ac.uk
[2] Institute of Physics, Nonlinear Dynamics Group, Universität Potsdam,
Germany

Summary. This chapter presents an introductory course to the biophysics of neurons, comprising a discussion of ion channels, active and passive membranes, action potentials and postsynaptic potentials. It reviews several conductance-based and reduced neuron models, neural networks and neural field theories. Finally, the basic principles of the neuroelectrodynamics of mass potentials, i.e. dendritic fields, local field potentials, and the electroencephalogram are elucidated and their putative functional role as a mean field is discussed.

1.1 Introduction

Metaphorically, the brain is often compared with a digital computer [1, 2] that runs *software* algorithms in order to perform cognitive computations. In spite of its usefulness as a working hypothesis in the cognitive [3–6] and computational [7–18] neurosciences, this metaphor does obviously not apply to the *hardware* level. Digital computers consist of circuit boards equipped with chips, transistors, resistors, capacitances, power supplies, and other electronic components wired together. Digital computation is essentially based on controlled switching processes in semiconductors which are nonlinear physical systems. On the other hand, brains consist to 80% of water contained in cells and also surrounding cells. How can this physical *wet-ware* substrate support computational dynamics? This question should be addressed in the present chapter. Starting from the physiological facts about neurons, their cell membranes, electrolytes, and ions [19–21], I shall outline the biophysical principles of neural computation [12, 13, 15, 18, 22–25] in parallel to those of computation in electronic circuits. Thus, the interesting physiological properties will be described by electric "equivalent circuits" providing a construction kit of building blocks that allow the modeling of membranes, single neurons, and eventually neural networks. This field of research is broadly covered by *computational neuroscience*. However, since this discipline also deals with more abstract approximations of real neurons (see Sect. 1.4.3) and with artificial

neural networks, I prefer to speak about *neurophysics*, i.e. the biophysics of real neurons.

The chapter is organized as a journey along a characteristic neuron where the stages are Sects. 1.2–1.4. Looking at Fig. 8.1 in Chap. 8, the reader recognizes the *cell bodies*, or *somata*, of three cortical neurons as the triangular knobs. Here, our journey will start by describing the microscopically observable membrane potentials. Membranes separating electrolytes with different ion concentrations exhibit a characteristic resting potential. In a corresponding equivalent circuit, this voltage can be thought of being supplied by a battery. Moreover, passive membranes act as a capacitance while their semipermeability with respect to particular kinds of ions leads to an approximately ohmic resistance. This property is due to the existence of leaky ion channels embedded in the cell membrane. At the neuron's axon hillock (trigger zone), situated at the base of the soma, the composition of the cell membrane changes. Here and along the axon, voltage-gated sodium and potassium channels appear in addition to the leakage channels, both making the membrane active and excitable. As we shall see, the equivalent circuit of the membrane allows for the derivation of the famous *Hodgkin-Huxley equations* of the *action potentials* which are the basic of neural *conductance models*. Traveling along the axon, we reach the presynaptic terminals, where the Hodgkin-Huxley equations have to be supplemented by additional terms describing the dynamics of voltage-gated calcium channels. Calcium flowing into the terminal causes the release of transmitter vesicles that pour their content of neurotransmitter into the synaptic cleft of a chemical synapse. Then, at the postsynapse, transmitter molecules dock onto receptor molecules, which indirectly open other ion channels. The kinetics of these reactions give rise to the *impulse response functions* of the postsynaptic membranes. Because these membranes behave almost passively, a linear differential equation describes the emergence of *postsynaptic potentials* by the convolution product of the postsynaptic pulse response with the *spike train*, i.e. the sequence of action potentials. Postsynaptic potentials propagate along the *dendrites* and the soma of the neuron and superimpose linearly to a resulting signal that eventually arrives at the axon hillock, where our journey ends.

In Sect. 1.5, we shall change our perspective from the microscopic to the macroscopic. Here, the emergence of mass potentials such as the local field potential (LFP) and the electroencephalogram (EEG) will be discussed.

1.2 Passive Membranes

Neurons are cells specialized for the purpose of fast transfer and computation of information in an organism. Like almost every other cell, they posses a cell body containing a nucleus and other organelles and they are surrounded by a membrane separating their interior from the extracellular space. In order to collect information from their environment, the soma of a characteristic

neuron branches out into a *dendritic tree* while another thin process, the *axon*, provides an output connection to other neurons [19–21]. The cell plasma in the interior as well as the liquid in the extracellular space are electrolytes, i.e. solutions of different kinds of ions such as sodium (Na^+), potassium (K^+), calcium (Ca^{2+}), chloride (Cl^-), and large organic ions. However, the concentrations of these ions (denoted by $[Na^+], [K^+], [Ca^{2+}]$, etc.) can differ drastically from one side of the cell membrane to the other (see Fig. 2.1 of Chap. 2). Therefore, the membrane is subjected to two competing forces: the osmotic force aiming at a compensation of these concentration gradients on the one hand, and the Coulomb force aiming at a compensation of the electric potential gradient. Biochemically, cell membranes are lipid bi-layers swimming like fat blobs in the plasma soup [19, 20], which makes them perfect electric isolators. Putting such a dielectric between two opposite electric charges yields a capacitance of capacity

$$C_m = \frac{Q}{U}\,, \tag{1.1}$$

where Q is the total charge stored in the capacitance and U is the voltage needed for that storage. Hence, a membrane patch of a fixed area A that separates different ion concentrations can be represented by a single capacitance $C_m = 1\,\mu\mathrm{F\,cm^{-1}} \times A$ in an equivalent "circuit" shown in Fig. 1.1 [19, 20].

Generally, we interpret such equivalent circuits in the following way: The upper clamp refers to the extracellular space whereas the clamp at the bottom measures the potential within the cell. Due to its higher conductance, the extracellular space is usually assumed to be equipotential, which can be designated as $U = 0\,\mathrm{mV}$ without loss of generality.

1.2.1 Ion Channels

If neuron membranes were simply lipid bi-layers, there would be nothing more to say. Of course, they are not. All the dynamical richness and computational complexity of neurons is due to the presence of particular proteins, called *ion channels*, embedded in the cell membranes. These molecules form tubes traversing the membrane that are permeable to certain kinds of ions [19–25]. The "zoo" of ion channels is comparable with that of elementary particles. There are channels whose pores are always open (*leakage channels*) but permeable only for sodium or potassium or chloride. Others possess *gates* situated in their pores which are controlled by the membrane potential, or the presence of certain substances or even both. We shall refer to the first kind of channels as to *voltage-gated channels*, and to the second kind as to *ligand-gated*

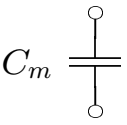

Fig. 1.1. Equivalent "circuit" for the capacitance C_m of a membrane patch

channels. Furthermore, the permeability of a channel can depend on the direction of the ionic current such that it behaves as a rectifier whose equivalent "circuit" would be a diode [19, 20]. Eventually, the permeability could be a function of the concentration of particular reagents either in the cell plasma or in the extracellular space, which holds not only for ligand-gated channels. Such substances are used for classifying ion channels. Generally, there are two types of substances. Those from the first class facilitate the functioning of a channel and are therefore called *agonists*. The members of the second class are named *antagonists* as they impede channel function.

Omitting these complications for a while, we assume that a single ion channel of kind k behaves as an ohmic resistor with conductance

$$\gamma_k = \frac{1}{\rho_k}\,, \tag{1.2}$$

where ρ_k is the resistivity of the channel. A typical value (for the gramicidin-A channel) is $\gamma_{\mathrm{GRAMA}} \approx 12\,\mathrm{pS}$. Figure 1.2 displays the corresponding equivalent "circuit".

In the remainder of this chapter, we will always consider membrane patches of a fixed area A. In such a patch, many ion channels are embedded, forming the parallel circuit shown in Fig. 1.3(a).

According to Kirchhoff's First Law, the total conductance of the parallel circuit is

$$g_k = N_k \gamma_k \tag{1.3}$$

when N_k channels are embedded in the patch, or, equivalently, expressed by the channel concentration $[k] = N_k/A$,

$$g_k = [k] A \gamma_k\,.$$

1.2.2 Resting Potentials

By embedding leakage channels into the cell membrane, it becomes *semipermeable*, i.e. permeable for certain kinds of ions while impenetrable for others. If there is a concentration gradient of a permeable ion across a semipermeable membrane, a diffusion current I_{diff} through the membrane patch A is created, whose density obeys Fick's Law

$$j_{\mathrm{diff}} = -D\, q \frac{\mathrm{d[I]}}{\mathrm{d}x}\,, \tag{1.4}$$

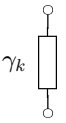

Fig. 1.2. Equivalent "circuit" for a single ohmic ion channel with conductance γ_k

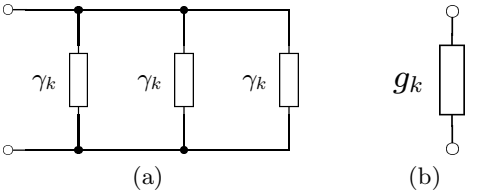

Fig. 1.3. Equivalent circuits (**a**) for ion channels of one kind k connected in parallel; (**b**) Substituted by a single resistor of conductance $g_k = 3\gamma_k$

where $\mathrm{d[I]}/\mathrm{d}x$ denotes the concentration gradient for ion I, q its charge, and $D = k_\mathrm{B}T/\mu$ is the diffusion constant given by Einstein's relation [26] (k_B is Boltzmann's constant, T is the temperature and μ is the viscosity of the electrolyte) [22–25]. This diffusion current can be described by an equivalent "circuit" given by a current source I_diff (Fig. 1.4).

The separation of charges by the diffusion current leads to an increasing potential gradient $\mathrm{d}U/\mathrm{d}x$ across the membrane. Therefore, a compensating ohmic current

$$j_\mathrm{ohm} = -\sigma \frac{\mathrm{d}U}{\mathrm{d}x} \tag{1.5}$$

flows back through the leakage channels ($\sigma = q^2[\mathrm{I}]/\mu$ is the conductance of the electrolyte expressed by the ion concentration and its charge). Then the total current $j = j_\mathrm{diff} + j_\mathrm{ohm}$ (visualized by the circuit in Fig. 1.5) is described by the *Nernst-Planck equation*

$$j = -D\, q \frac{\mathrm{d[I]}}{\mathrm{d}x} - [\mathrm{I}]\, \frac{q^2}{\mu}\, \frac{\mathrm{d}U}{\mathrm{d}x}\,. \tag{1.6}$$

The Nernst Equation

The general quasi-stationary solution of (1.6), the Goldman-Hodgkin-Katz equation ((2.4) in Chap. 2), clearly exhibits a nonlinear dependence of the ionic current on the membrane voltage [22–25]. However, for only small deviations from the stationary solution — given by the *Nernst equation*

$$E_\mathrm{I} = \frac{k_\mathrm{B}T}{q}\, \ln \frac{[\mathrm{I}]_\mathrm{out}}{[\mathrm{I}]_\mathrm{int}}\,, \tag{1.7}$$

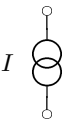

Fig. 1.4. Equivalent "circuit" either for the diffusion currents through the cell membrane or for the active ion pumps

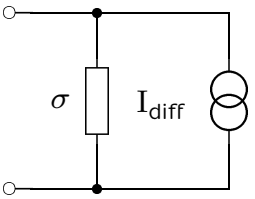

Fig. 1.5. Equivalent circuit for the derivation of the Nernst-Planck equation (1.6)

where $[\mathrm{I}]_{\mathrm{out}}$ is the ion concentration in the extracellular space and $[\mathrm{I}]_{\mathrm{int}}$ within the cell — the current can be regarded as being ohmic.

For room temperature, the factor $k_{\mathrm{B}}T/q \approx 25\,\mathrm{mV}$. With the concentrations from Fig. 2.1, Chap. 2, this leads to the characteristic resting potentials; e.g. $U_{\mathrm{K}^+} = -101\,\mathrm{mV}$, and $U_{\mathrm{Na}^+} = +56\,\mathrm{mV}$.

Each sort of ion possesses its own Nernst equilibrium potential. We express this fact by a battery in an equivalent "circuit" shown in Fig. 1.6.

Now, we are able to combine different ion channels k all selective for one sort of ions I with their corresponding power supplies. This is achieved by a serial circuit as shown in Fig. 1.7. This equivalent circuit will be our basic building block for all other subsequent membrane models.

If the clamp voltage of this circuit has the value U, we have to distribute this voltage according to Kirchhoff's Second Law as

$$U = \frac{I_k}{g_k} + E_{\mathrm{I}}\,,$$

leading to the fundamental equation

$$I_k = g_k(U - E_{\mathrm{I}})\,. \tag{1.8}$$

The Goldman Equation

As an example, we assume that three types of ion channels are embedded in the membrane patch, one pervious for sodium with the conductance g_{Na^+}, another pervious for potassium with the conductance g_{K^+}, and the third pervious for chloride with the conductance g_{Cl^-}, respectively. Figure 1.8 displays the corresponding equivalent circuit.

Interpreting the top of the circuit as the extracellular space and the bottom as the interior of the neuron, we see that the resting potential for potassium

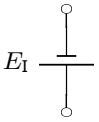

Fig. 1.6. Equivalent circuit for the Nernst equilibrium potential (1.7)

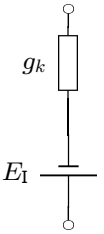

Fig. 1.7. Equivalent circuit for a population of ion channels of kind k selective for the ion sort I embedded in a membrane with resting potential E_I

and chloride is negative (denoted by the short tongue of the battery symbol) while the sodium equilibrium potential is positive in comparison to the extracellular space.

According to Kirchhoff's First Law, the total current through the circuit is

$$I = I_{\mathrm{Na}^+} + I_{\mathrm{K}^+} + I_{\mathrm{Cl}^-} \,. \tag{1.9}$$

To obtain the stationary equilibrium, we have to set $I = 0$. Using the fundamental equation (1.8), we get the equation

$$0 = g_{\mathrm{Na}^+}(U - E_{\mathrm{Na}^+}) + g_{\mathrm{K}^+}(U - E_{\mathrm{K}^+}) + g_{\mathrm{Cl}^-}(U - E_{\mathrm{Cl}^-}) \,,$$

whose resolution entails the equilibrium potential

$$U = \frac{g_{\mathrm{Na}^+}E_{\mathrm{Na}^+} + g_{\mathrm{K}^+}E_{\mathrm{K}^+} + g_{\mathrm{Cl}^-}E_{\mathrm{Cl}^-}}{g_{\mathrm{Na}^+} + g_{\mathrm{K}^+} + g_{\mathrm{Cl}^-}} \,. \tag{1.10}$$

Equation (1.10) is closely related to the Goldman equation that can be derived from the Goldman-Hodgkin-Katz equation [24]. It describes the net effect of all leakage channels. Therefore, the circuit in Fig. 1.8 can be replaced by the simplification found in Fig. 1.9.

Accordingly, the leakage current is again given by (1.8)

$$I_l = g_l(U - E_l) \,. \tag{1.11}$$

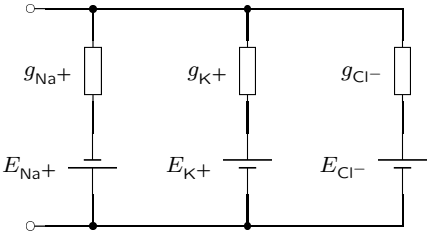

Fig. 1.8. Equivalent circuit for three populations of ion channels permeable for sodium, potassium and chloride with their respective Nernst potentials

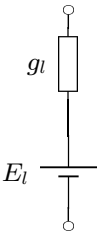

Fig. 1.9. Equivalent circuit for the total leakage current and its corresponding leakage potential E_l

Characteristic values are $g_l = 13\,\mu\text{S}$ for the leakage conductance and $E_l = -69\,\text{mV}$ for the leakage potential as the solution of (1.10) [19, 20].

While the Nernst potential for one kind of ions denotes a stationary state, the Goldman equilibrium potential results from a continuous in- and outflow of ions that would cease when all concentration gradients had been balanced. To stabilize the leakage potential the cell exploits active *ion pumps* modeled by a current source as displayed in Fig. 1.4. These ion pumps are proteins embedded in the cell membrane that transfer ions against their diffusion gradients by consuming energy. Maintaining resting potentials is one of the energetically most expensive processes in the nervous system [27]. This consumption of energy is, though rather indirectly, measurable by neuroimaging techniques such as positron emission tomography (PET) or functional magnetic resonance imaging (fMRI) [19, 20, 28, 29].

1.3 Active Membranes

The resting potentials we have discussed so far are very sensitive to changes in the conductances of the ion channels. While these are almost constant for the leakage channels, there are other types of channels whose conductances are functions of certain parameters such as the membrane potential or the occurrence of particular reagents. These channels make membranes active and dynamic. The former are called voltage-gated whereas the latter are referred to as ligand-gated. Basically, these channels occur in two dynamical states: their pore may be open (O) or closed (C). The conductance of closed channels is zero, while that of an open channel assumes a particular value γ_k. Therefore, a single gated channel can be represented by a serial circuit of a resistor with conductance γ_k and a switch S, as depicted in Fig. 1.10.

Let N_k be the number of gated channels of brand k embedded in our membrane patch of area A, and let O_k and C_k the number of momentarily open and closed channels of this kind, respectively. As argued in Sect. 1.2.1, the total conductance of all open channels is given by Kirchhoff's First Law as

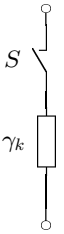

Fig. 1.10. Equivalent circuit for a single gated channel with open-conductance γ_k

$$g_k = O_k \, \gamma_k \, , \tag{1.12}$$

while

$$\bar{g}_k = N_k \, \gamma_k \tag{1.13}$$

is now the maximal conductance of these channels.

1.3.1 Action Potentials

Signals propagate mainly passively along the dendritic and somatic membranes until they reach the axon hillock, or trigger zone of the neuron. Here, the composition of the membrane changes significantly and voltage-gated sodium and potassium channels supplement the all-pervasive leakage channels. Above, we have modeled these channels by switches connected serially with ohmic resistors. Now, the crucial question arises: Who opens the switches?

Here, for the first time, a stochastic account is required. Ion channels are macro-molecules and hence quantum objects. Furthermore, these objects are weakly interacting with their environments. Therefore the cell membrane and the electrolytes surrounding it provide a *heat bath* making a thermodynamical treatment necessary. From a statistical point of view, an individual channel has a probability of being open, p_k, such that the number of open channels is the expectation value

$$O_k = p_k \, N_k \, . \tag{1.14}$$

Inserting (1.14) into (1.12) yields the conductance

$$g_k = p_k \, N_k \, \gamma_k = p_k \, \bar{g}_k \, . \tag{1.15}$$

The problem of determining the probability p_k is usually tackled by modeling Markov chains [24, 25]. The simplest approach is a two-state Markov process shown in Fig. 1.11, where C and O denote the closed and the open state, respectively, while α, β are transition rates.

The state probabilities of the Markov chain in Fig. 1.11 obey a *master equation* [30, 31]

$$\frac{\mathrm{d}p_k}{\mathrm{d}t} = \alpha_k \, (1 - p_k(t)) - \beta_k \, p_k(t) \, , \tag{1.16}$$

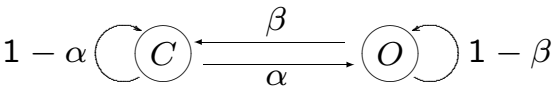

Fig. 1.11. Two-state Markov model of a voltage-gated ion channel

whose transition rates are given by the thermodynamic Boltzmann weights

$$\alpha_k = \mathrm{e}^{\frac{W(C\to O)}{k_\mathrm{B}T}}\,, \tag{1.17}$$

where $W(C \to O)$ is the necessary amount of energy that has to be supplied by the heat bath to open the channel pore.

Channel proteins consist of amino acids that are to some extent electrically polarized [19–21]. The gate blocking the pore is assumed to be a subunit with charge Q. Call $W_0(C \to O)$ the work that is necessary to move Q through the electric field generated by the other amino acids to open the channel pore. Superimposing this field with the membrane potential U yields the total transition energy

$$W(C \to O) = W_0(C \to O) + QU\,. \tag{1.18}$$

If $QU < 0$, $W(C \to O)$ is diminished and the transition $C \to O$ is facilitated [12], thereby increasing the rate α_k according to

$$\alpha_k(U) = \mathrm{e}^{\frac{W_0(C\to O)+QU}{k_\mathrm{B}T}}\,. \tag{1.19}$$

The equations (1.15, 1.16, 1.19) describe the functioning of voltage-gated ion channels [12,13,15,23–25]. Yet, voltage-gated resistors are also well-known in electric engineering: *transistors* are *transi*ent resi*stors*. Though not usual in the literature, I would like to use the transistor symbol to denote voltage-gated ion channels here (Fig. 1.12). In contrast to batteries, resistors and capacitors, which are *passive* building blocks of electronic engineering, transistors are *active* components thus justifying our choice for active membranes.

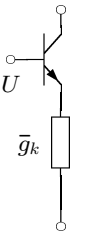

Fig. 1.12. Equivalent circuit for a population of voltage-gated ion channels. The maximal conductance $\bar{g}_k$ is reached when the transistor is in saturation

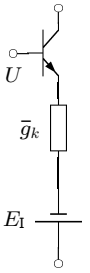

Fig. 1.13. Equivalent circuit for a population of voltage-gated ion channels of kind k selective for the ion sort I embedded in a membrane with resting potential E_I

Corresponding to Fig. 1.7, the equivalent circuit for a population of voltage-gated channels of kind k permeable for ions I supplied by their respective resting potential E_I is provided in Fig. 1.13.

The Hodgkin-Huxley Equations

Now we are prepared to derive the Nobel-prize-winning Hodgkin-Huxley equations for the action potential [32] (see also [12–15, 23–25]). Looking again at Fig. 1.8, one easily recognizes that an increase of the sodium conductance leads to a more positive membrane potential, or, to a *depolarization*, while an increasing conductance either of potassium or of chloride entails a further negativity, or *hyperpolarization* of the membrane potential. These effects are in fact achieved by voltage-gated sodium and potassium channels which we refer here to as AN and AK, respectively. Embedding these into the cell membrane yields the equivalent circuit shown in Fig. 1.14.[3]

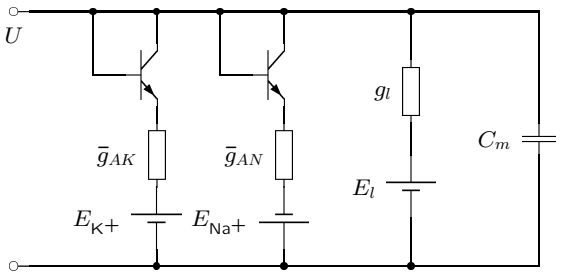

Fig. 1.14. Equivalent circuit for the Hodgkin-Huxley equations (1.25, 1.27–1.29)

[3] I apologize to all electrical engineers for taking their notation rather symbolically. Certainly, this circuit has neither protection resistors nor voltage stabilizers and should not be reproduced. Sorry for that!

The first and second branches represent the voltage-gated potassium and sodium channels, respectively. The third is taken from the stationary descriptions of the leakage potential (Sect. 1.2.2) while the capacitance is now necessary to account for the dynamics of the membrane potential. According to Kirchhoff's First Law, the total current through the circuit adds up to an injected current I_m,

$$I_m = I_{AK} + I_{AN} + I_l + I_C \,. \tag{1.20}$$

The partial currents are

$$I_{AK} = p_{AK}\, \bar{g}_{AK}(U - E_{\mathrm{K}^+}) \tag{1.21}$$

$$I_{AN} = p_{AN}\, \bar{g}_{AN}(U - E_{\mathrm{Na}^+}) \tag{1.22}$$

$$I_l = g_l(U - E_l) \tag{1.23}$$

$$I_C = C_m \frac{\mathrm{d}U}{\mathrm{d}t} \,, \tag{1.24}$$

where (1.21, 1.22) are produced from (1.15) and (1.8), (1.23) is actually (1.11) and (1.24) is the temporal derivative of (1.1). Taken together, the membrane potential $U(t)$ obeys the differential equation

$$C_m \frac{\mathrm{d}U}{\mathrm{d}t} + p_{AK}\, \bar{g}_{AK}(U - E_{\mathrm{K}^+}) + p_{AN}\, \bar{g}_{AN}(U - E_{\mathrm{Na}^+}) + g_l(U - E_l) = I_m \,. \tag{1.25}$$

Equation (1.25) has to be supplemented by two master equations: (1.16) for the open probabilities p_{AK}, p_{AN} and the rate equations (1.19) for α_{AK}, α_{AN}.

Unfortunately, this approach is inconsistent with the experimental findings of Hodgkin and Huxley [32]. They reported two other relations

$$p_{AK} = n^4; \qquad p_{AN} = m^3\, h \,, \tag{1.26}$$

where n, m and h now obey three master equations

$$\frac{\mathrm{d}n}{\mathrm{d}t} = \alpha_n\,(1 - n) - \beta_n\, n \tag{1.27}$$

$$\frac{\mathrm{d}m}{\mathrm{d}t} = \alpha_m\,(1 - m) - \beta_m\, m \tag{1.28}$$

$$\frac{\mathrm{d}h}{\mathrm{d}t} = \alpha_h\,(1 - h) - \beta_h\, h \,. \tag{1.29}$$

The equations (1.25, 1.27–1.29) are called Hodgkin-Huxley equations [12–15, 23–25, 32]. They constitute a four-dimensional nonlinear dynamical system controlled by the parameter I_m. Figure 1.15 displays numerical solutions for three different values of I_m.

Figure 1.15 illustrates only two of a multitude of dynamical patters of the Hodgkin-Huxley system. Firstly, it exhibits a threshold behavior that is due to a Hopf bifurcation [18]. For subthreshold currents (solid line: $I_m = 7.09\,\mu\mathrm{A}$), one observes a damped oscillation corresponding to a stable fixed point in

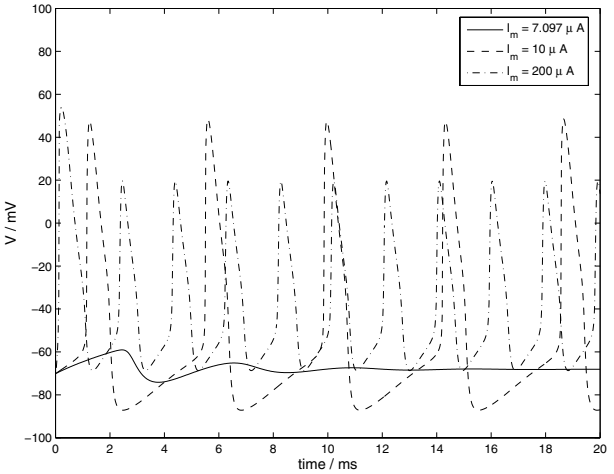

Fig. 1.15. Numeric solutions of the Hodgkin-Huxley equations (1.25, 1.27–1.29) according to the Rinzel-Wilson model (Sect. 1.4.3) for three different values of the control parameter I_m. *Solid: subthreshold current* $I_m = 7.09\,\mu$A; *dashed: superthreshold current* $I_m = 10\,\mu$A; *dashed-dotted: even higher current* $I_m = 200\,\mu$A

the phase space. If the control parameter I_m exceeds a certain threshold θ, this fixed point destabilizes and a limit cycle emerges (dashed line: $I_m = 10\,\mu$A). Secondly, further heightening of I_m leads to limit cycles of increased frequencies (dashed-dotted line: $I_m = 200\,\mu$A). This *regular spiking* dynamics explains the law of all-or-nothing as well as the encoding principle by frequency modulation in the nervous system [19–21].

In order to interpret the Hodgkin-Huxley equations (1.25, 1.27–1.29) biologically, we have to consider (1.26) first. It tells that our simple two-state Markov chain (Fig. 1.11) is not appropriate. Instead, the description of the active potassium channel requires a four-state Markov chain comprising three distinct closed and one open state [24, 25]. However, (1.26) allows for another instructive interpretation: According to a fundamental theorem of probability theory, the joint probability of disjunct events equals the product of the individual probabilities upon their stochastic independence. Since $p_{AK} = n^4$, we can assume the existence of four independently moving *gating charges* within the channel molecule. Correspondingly, for the sodium channel we expect three independent gating charges and one inhibiting subunit since $p_{AN} = m^3\,h$. This is supported by patch clamp measurements where the channel's pores were blocked by the Fugu's fish tetradotoxin [19–21]. Although the blocked channel could not pass any ions, about three brief currents were observed. We can imagine these charges as key cylinders that have to be brought into the right positions to unlock a cylinder lock (thus opening the channel).

The emergence of an action potential results from different kinetics of the ion channels. If the cell membrane is slightly depolarized by the current I_m,

the opening rate α_n for the sodium channels increases, thus entailing a further depolarization of the membrane. The positive feed-back loop started in this way leads to a torrent of inflowing sodium until the peak of the action potential is reached. Then, the membrane potential is positive in comparison to the extracellular space, causing voltage-gated potassium channels to open. Due to its negative equilibrium potential, potassium leaves the cell thereby hyperpolarizing the interior. Contrastingly, the hyperpolarization of the membrane reduces the open probability of the sodium channels, which become increasingly closed. Another positive feed-back loop enhances the hyperpolarization thereby overshooting the resting potential. While the potassium channels change very slowly back to their closed state, the sodium channels become additionally inactivated by a stopper subunit of the channel molecule whose kinetics is governed by the h term. This inhibition process is responsible for the refractory time prohibiting the occurrence of another action potential within this period.

1.3.2 Presynaptic Potentials

A spike train, generated in the way described by the Hodgkin-Huxley equations, travels along the axon and, after several branches, reaches the presynaptic terminals. Here, the composition of the membrane changes again. Voltage-gated calcium channels are present in addition to the voltage-gated potassium and sodium channels, and can be described by another branch in Fig. 1.14. The class of voltage-gated calcium channels is quite extensive and they operate generally far from the linear (ohmic) domain of the Goldman-Hodgkin-Katz equation [13, 15, 24, 25]. However, according to Johnston & Wu [24], an ohmic treatment of presynaptic Ca^{2+} channels is feasible such that their current is given by

$$I_{AC} = l^5\, \bar{g}_{AC}\, (U - E_{Ca^{2+}})\,, \tag{1.30}$$

where l obeys another master equation

$$\frac{\mathrm{d}l}{\mathrm{d}t} = \alpha_l\, (1 - l) - \beta_l\, l\,. \tag{1.31}$$

In the absence of an injected current ($I_m = 0$), the presynaptic potential $U(t)$ is then governed by the differential equation

$$C_m \frac{\mathrm{d}U}{\mathrm{d}t} + I_{AK} + I_{AN} + I_{AC} + I_l = 0\,. \tag{1.32}$$

Neglecting calcium leakage, the current (1.30) leads to an enhancement of the intracellular concentration $[Ca^{2+}]_{\mathrm{int}}$ that is described by a continuity equation [12]

$$\frac{\mathrm{d}[Ca^{2+}]_{\mathrm{int}}}{\mathrm{d}t} = -\frac{I_{AC}}{qN_{\mathrm{A}}V}\,. \tag{1.33}$$

Here, $q = 2e$ is the charge of the calcium ion (e denoting the elementary charge). Avogadro's constant N_A scales the ion concentration to moles contained in the volume V. The accumulation of calcium in the cell plasma gives rise to a cascade of metabolic reactions. Calcium does not only serve as an electric signal; it also acts as an important messenger and chemical reagent, enabling or disenabling the functioning of enzymes.

The movement of neurotransmitter into the synaptic cleft comprises two sub-processes taking place in the presynaptic terminal: Firstly, transmitter must be allocated, and secondly, it must be released. The allocation of transmitter depends on the intracellular calcium concentration (1.33), while it is stochastically released by increased calcium currents (1.30) as a consequence of an arriving action potential with a probability p.

In the resting state, transmitter vesicles are anchored at the cytoskeleton by proteins called *synapsin*, which act like a wheel clamp. The probability to loosen these joints increases with the concentration $[\mathrm{Ca}^{2+}]_\mathrm{int}$. Liberated vesicles wander to one of a finite number Z of *active zones* where vesicles can fuse with the terminal membrane thereby releasing their content into the synaptic cleft by the process of *exocytosis* [19–21]. Allocation means that $Y \leq Z$ active zones are provided with vesicles, where

$$Y = \kappa([\mathrm{Ca}^{2+}]_\mathrm{int})\, Z \tag{1.34}$$

is the average number of occupied active zones, and $\kappa([\mathrm{Ca}^{2+}]_\mathrm{int})$ is a monotonic function of the calcium concentration that must be determined from the reaction kinetics between calcium and synapsin mediated by kinases. The release of transmitter is then described by a *Bernoulli process* started by an arriving action potential. The probability that k of the Y occupied active zones release a vesicle is given by the *binomial distribution*

$$p(k, Y) = \binom{Y}{k} p^k (1-p)^{Y-k}\,. \tag{1.35}$$

For the sake of mathematical convenience, we shall replace the binomial distribution by a normal distribution

$$\rho(k, Y) = \frac{1}{\sqrt{2\pi y(1-p)}} \exp\left[-\frac{(k-y)^2}{2y(1-p)}\right], \tag{1.36}$$

where $y = Yp$ is the average number of transmitter releasing active zones. Assuming that a vesicle contains on average $n_T = 5000$ transmitter molecules [19, 20], we can estimate the mean number of transmitter molecules that are released by an action potential as

$$T = n_T Y p = n_T Z p\, \kappa([\mathrm{Ca}^{2+}]_\mathrm{int})\,. \tag{1.37}$$

Correspondingly, the expected number of transmitter molecules released by k vesicles is given by

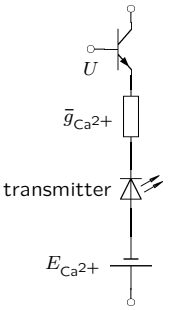

Fig. 1.16. Equivalent circuit for the calcium-controlled transmitter release (indicated by the arrows of the LED)

$$T(k) = \frac{n_T Y}{\sqrt{2\pi y(1-p)}} \exp\left[-\frac{(k-y)^2}{2y(1-p)}\right]. \tag{1.38}$$

Finally, we need an equivalent circuit symbol for the transmitter release. Electronics suggests the use of the LED symbol (light-emitting diode). Connected all together, the calcium controlled transmitter release might be represented by the branch shown in Fig. 1.16.

1.3.3 Postsynaptic Potentials

After being poured out into the synaptic cleft of a chemical synapse, transmitter molecules diffuse to the opposite postsynaptic membrane, unless they have not been decomposed by enzymic reactions. There, they dock onto *receptor molecules*, which fall into two classes: *ionotropic receptors* are actually transmitter-gated ion channels, whereas *metabotropic receptors* are proteins that, once activated by transmitter molecules, start metabolic processes from second messenger release up to gene expression. At particular pathways, they control the opening of other ion channels gated by intracellular reaction products. The directly transmitter-gated channels are fast and effective, while the intracellularly gated channels react very slowly [19–21, 33]. In this section, I shall treat two distinct examples from each receptor class.

Excitatory Postsynaptic Potentials

One important transmitter-gated ion channel is (among others, such as the AMPA, $GABA_A$, and NMDA receptors) the nACh receptor that has nicotine as an antagonist. It becomes open if three or four molecules of the neurotransmitter acetylcholine (ACh) dock at its surface rising into the synaptic cleft. These molecules cause shifts of the electric polarization within the molecule which opens the gate in the pore. This process can be modeled by a Markov chain similarly to the exposition in Sect. 1.3.1. However, another treatment is also feasible, using *chemical reaction networks* [30, 33].

The open nACh channel is conductive for sodium as well as for potassium ions, such that its reversal (resting) potential is provided by the Goldman equation (1.10). Yet the sodium conductance is slightly larger than that for potassium yielding a net current of inflowing sodium ions. Since this current is depolarizing, the nACh channels constitute *excitatory synapses*. Therefore, they generate *excitatory postsynaptic potentials* (EPSP). On the other hand, hyperpolarizing channels, such as the $\mathrm{GABA_A}$ channel, constitute *inhibitory synapses* generating *inhibitory postsynaptic potentials* (IPSP).

Let us once more consider a membrane patch of area A containing N_{nACh} receptors. Again, let O_{nACh} be the number of momentarily opened and C_{nACh} the number of closed channels. According to (1.12), the conductance of all open channels connected in parallel is then $g_{\mathrm{nACh}} = O_{\mathrm{nACh}}\,\gamma_{\mathrm{nACh}}$. Opening of the channels can now be described by the *chemical reaction equation*

$$C + 3T \rightleftarrows O\,, \tag{1.39}$$

where C denotes the closed and O the opened molecules. T stands for the transmitter ACh. Because in each single reaction, three molecules T react with one molecule C to produce one molecule O, the corresponding *kinetic equation* [30, 31, 33] comprises a cubic nonlinearity,

$$\frac{\mathrm{d}O}{\mathrm{d}t} = \nu_1 C T^3 - \nu_2 O\,, \tag{1.40}$$

where ν_1 denotes the production and ν_2 the decomposition rate of open channels in (1.39). These reaction rates depend on the temperature of the heat bath and probably on metabolic circumstances such as phosphorylation. This equation has to be supplemented by a *reaction-diffusion equation* for the neurotransmitter reservoir in the synaptic cleft

$$\frac{\mathrm{d}T}{\mathrm{d}t} = \nu_2 O - \nu_3 T E - \sigma T\,, \tag{1.41}$$

where $\nu_2 O$ is the intake of transmitter due to decaying receptor-transmitter complexes, which is the same as the loss of open channels in (1.40), $\nu_3 TE$ is the decline due to reactions between the transmitter with enzyme E, and σT denotes the diffusion out of the synaptic cleft. Its initial condition $T(t = 0)$ is supplied by (1.38). Taken together, the equations (1.40, 1.41) describe the *reaction-diffusion kinetics* of the ligand-gated ion channel nACh.

Expressing the electric conductivity (1.12) through the maximal conductivity $\bar{g}_{\mathrm{nACh}}$,

$$g_k = \frac{O_{\mathrm{nACh}}}{N_{\mathrm{nACh}}}\,\bar{g}_{\mathrm{nACh}}\,, \tag{1.42}$$

suggests a new equivalent circuit symbol for ligand-gated channels. The conductance is controlled by the number of transmitter molecules, i.e. the number of particular particles in the environment. This corresponds to the phototransistor in electronic engineering which is controlled by the number of photons

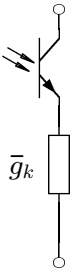

Fig. 1.17. Equivalent circuit for a population of ligand-gated ion channels of kind k

collected by its base. Hence, I would like to suggest the circuit shown in Fig. 1.17 as an equivalent to the nACh receptor.

In order to compute the postsynaptic potential, the circuit in Fig. 1.17 has to be connected in parallel with the leakage conductance and the membrane capacitance as in Fig. 1.18.

The EPSP for the nACh receptor then obeys the equations

$$C_m \frac{\mathrm{d}U}{\mathrm{d}t} + \frac{O_{\mathrm{nACh}}}{N_{\mathrm{nACh}}} \bar{g}_{\mathrm{nACh}}(U - E_{\mathrm{nACh}}) + g_l(U - E_l) = 0 \tag{1.43}$$

together with (1.40, 1.41), and initial condition (1.38).

However, instead of solving these differential equations, most postsynaptic potentials can be easily described by alpha functions as synaptic gain functions [12–16, 18]

$$U^{\mathrm{PSP}}(t) = E_{\mathrm{PSP}}\, \alpha^2 t\, \mathrm{e}^{-\alpha t}\, \Theta(t)\,, \tag{1.44}$$

where α is the characteristic time constant of the postsynaptic potential (PSP) and

$$\Theta(t) = \begin{cases} 0 & \text{for} \quad t \leq 0 \\ 1 & \text{for} \quad t > 0 \end{cases} \tag{1.45}$$

is Heaviside's jump function.

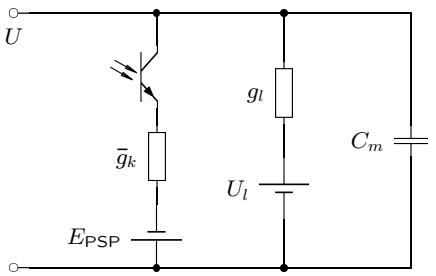

Fig. 1.18. Equivalent circuit for the postsynaptic potential generated by ligand-gated channels of kind k with reversal potential PSP

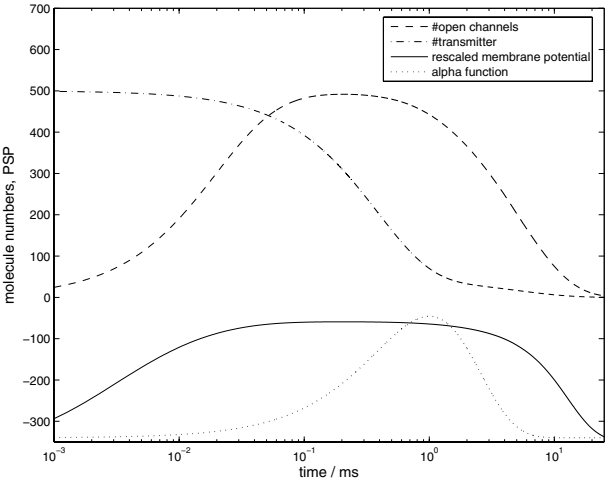

Fig. 1.19. Numeric solutions of the kinetic equations (1.40, 1.41, 1.43) for the nACh receptor. *Dashed-dotted*: the number of ACh molecules (max = 500); *dashed*: the number of open nACh channels (max = 500); *solid*: the EPSP $U(t)$; *dotted*: an alpha function (1.44). The time axis is logarithmically scaled; the functions are rescaled and (if necessary) shifted for better visibility

Figure 1.19 displays the numerical solution of equations (1.40, 1.41, 1.43) for arbitrarily chosen parameters together with a "fitted" alpha function for comparison. Obviously, the correspondence is not that large.

Inhibitory Postsynaptic Potentials

Synapses are excitatory if they open sodium or calcium channels with more positive reversal potentials compared to the resting state. Their neurotransmitters are generally acetylcholine (ACh) or the amino acid glutamate. Contrastingly, most inhibitory synapses employ the amino acids glycine or GABA (gamma-amino-butyric-acid) to open potassium or chloride channels with more negative reversal potentials. While the $\mathrm{GABA_A}$ receptor is transmitter-gated such as the nACh receptor discussed in the previous section, the $\mathrm{GABA_B}$- and mACh receptors (having the toadstool toxin *muscarine* as an antagonist) activate intracellular *G proteins* which subsequently open G protein-gated potassium channels [19–21]. The activation of G protein-gated potassium channels comprises the following chemical reactions [12]:

$$\begin{aligned} R_0 + T &\rightleftarrows R^* \rightleftarrows D \\ R^* + G_0 &\rightleftarrows RG^* \rightarrow R^* + G^* \\ G^* &\rightarrow G_0 \\ C + n\,G^* &\rightleftarrows O\,, \end{aligned} \tag{1.46}$$

where R_0 is the metabotropic $\mathrm{GABA_B}$ receptor in its resting state, T the transmitter GABA, R^* the transmitter-activated receptor on the one hand, and D the same transmitter-receptor complex in its inactivated state on the other hand; furthermore, G_0 is the G protein in its resting state, $(RG)^*$ a short-lived activated receptor-G protein complex and G^* the activated G protein; finally, C is the G protein-gated potassium channel in its closed state and O in the open state. The channel possesses n docking sites for G protein molecules. Translating (1.46) into kinetic equations and adding (1.41) yields

$$\frac{\mathrm{d}R_0}{\mathrm{d}t} = -\nu_1\, R_0 T + \nu_2\, R^* \tag{1.47}$$

$$\frac{\mathrm{d}T}{\mathrm{d}t} = -\nu_1\, R_0 T + \nu_2\, R^* - \nu_{11}\, TE - \sigma T \tag{1.48}$$

$$\begin{aligned}\frac{\mathrm{d}R^*}{\mathrm{d}t} &= \nu_1\, R_0 T - \nu_2\, R^* + \nu_3\, D - \nu_4 R^* \\ &\quad -\nu_5\, R^* G_0 + \nu_6\, (RG)^* + \nu_8\, (RG)^*\end{aligned} \tag{1.49}$$

$$\frac{\mathrm{d}D}{\mathrm{d}t} = -\nu_3\, D + \nu_4 R^* \tag{1.50}$$

$$\frac{\mathrm{d}G_0}{\mathrm{d}t} = -\nu_5\, R^* G_0 + \nu_6\, (RG)^* + \nu_7\, G^* \tag{1.51}$$

$$\frac{\mathrm{d}(RG)^*}{\mathrm{d}t} = \nu_5\, R^* G_0 - \nu_6\, (RG)^* - \nu_8\, (RG)^* \tag{1.52}$$

$$\frac{\mathrm{d}G^*}{\mathrm{d}t} = -\nu_7\, G^* + \nu_8\, (RG)^* + \nu_{10}\, O \tag{1.53}$$

$$\frac{\mathrm{d}O}{\mathrm{d}t} = \nu_9\, C {G^*}^n - \nu_{10}\, O \tag{1.54}$$

for the metabolic dynamics. Equations (1.47–1.54) together with (1.43) describe the inhibitory GABA-ergic potential

$$C_m \frac{\mathrm{d}U}{\mathrm{d}t} + \frac{O}{O+C}\, \bar{g}_{\mathrm{GP}} (U - E_{\mathrm{K}^+}) + g_l (U - E_l) = 0\,, \tag{1.55}$$

where $\bar{g}_{\mathrm{GP}}$ denotes the maximal conductance and E_{K^+} the reversal potential of the G protein-gated potassium channels.

Temporal Integration

Each action potential arriving at the presynaptic terminal causes the (binomially distributed) release of one or more vesicles that pour their total amount of transmitter molecules into the synaptic cleft. Here, transmitter molecules react either with ionotropic or with metabotropic receptors which open — more or less directly — ion channels such that a postsynaptic current

$$I^{\mathrm{PSC}}(t) = \frac{O_k(t)}{N_k}\, \bar{g}_k (U - E_k)\,, \tag{1.56}$$

either excitatory or inhibitory, flows through the "phototransistor" branch of Fig. 1.17. This current gives rise to the EPSP or IPSP according to (1.43, 1.55). Since these potentials were determined for the transmitter released by one action potential, we can consider them as *impulse response functions*. Inserting I^{PSC} into (1.43, 1.55) and shifting the resting potential to $E_l = 0$ yields the inhomogeneous linear differential equation

$$\tau \frac{\mathrm{d}U}{\mathrm{d}t} + U = -\frac{I^{\mathrm{PSC}}}{C_m}\,, \tag{1.57}$$

with $\tau = C_m/g_l$ as the characteristic *time constant* of the membrane patch. If we describe the current I^{PSC} by a pulse of height I_0 at time t_0,

$$I^{\mathrm{PSC}}(t) = I_0 \delta(t - t_0)\,, \tag{1.58}$$

the solution of (1.57) is given by a Green's function $U^{\mathrm{PSP}} = G(t, t')$ [13,18,22]. By virtue of this Green's function, we can easily compute the postsynaptic potential evoked by an arbitrary spike train

$$I^{\mathrm{PSC}}(t) = I_0 \sum_k \delta(t - t_k) \tag{1.59}$$

as the *convolution product*

$$U^{\mathrm{PSP}}(t) = \int G(t, t')\, I^{\mathrm{PSC}}(t)\, \mathrm{d}t' = G * I^{\mathrm{PSC}}\,. \tag{1.60}$$

Inserting (1.59) into (1.60) gives

$$U^{\mathrm{PSP}}(t) = I_0 \sum_k G(t, t_k)\,. \tag{1.61}$$

If the action potentials are generated by the presynaptic neuron in the regular spiking mode with frequency f (see Sect. 1.3.1), the event times are given by

$$t_k = \frac{k}{f}\,. \tag{1.62}$$

Eventually, (1.61, 1.62) lead to

$$U^{\mathrm{PSP}}(t) = I_0 \sum_k G\left(t, \frac{k}{f}\right)\,. \tag{1.63}$$

Figure 1.20 displays two postsynaptic potentials obtained by the convolution of the Green's function

$$G(t, t') = \Theta(t - t') \cdot \frac{I_0}{C_m} \exp\left(-\frac{t - t'}{\tau}\right)$$

with regular spike trains.

By means of the convolution mechanism, an analogue continuously varying membrane potential is regained from a frequency-modulated spike train. This process is called *temporal integration*.

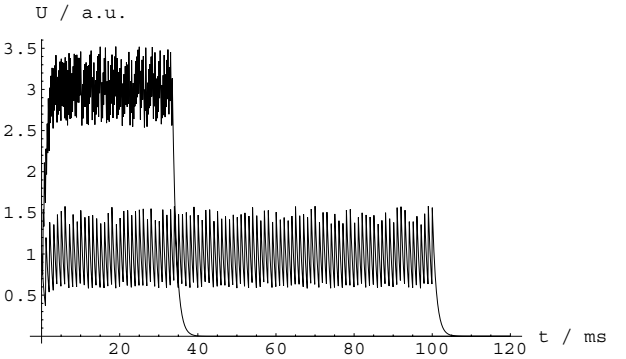

Fig. 1.20. Temporal integration of postsynaptic pulse responses for a lower (*lower curve*) and a higher regular spiking frequency (*upper curve*)

1.4 Neuron Models

In the preceding sections, we completed our construction kit for neurophysical engineering. In the remaining ones, we are going to apply these building blocks. There are three main threads of neural modeling. The first one builds point models, where all kinds of ion channels are connected in parallel. Secondly, compartment models additionally take into account the cable properties of cell membranes that are responsible for *spatial integration* processes. However, all these models are computationally very expensive. Therefore several simplifications and abstractions have been proposed to cope with these problems especially for the modeling of *neural networks*. Nevertheless, for the simulation of relatively small networks of point or compartment models, powerful software tools such as `GENESIS` [34], or `NEURON` [35] have been developed.

1.4.1 Point Models

In the point model account, all membrane patches of a nerve cell are assumed to be equipotential, disregarding its spacial extension [12, 15, 36, 37]. In our equivalent circuits, this assumption is reflected by connecting all different ion channels in parallel. Figure 1.21 shows such a point model.

In order to simulate the neuron in Fig. 1.21, all discussed differential equations are to be solved simultaneously. Neural networks then consist of many circuits of this form that are "optically" coupled, i.e. by the transmitter releasing and receiving devices at both ends of one circuit. The efficacy of the coupling between two neurons i and j is expressed by the *synaptic weight* w_{ij}. Physiologically, these weights depend on the maximal synaptic conductances $\bar{g}_{\mathrm{PSP}}$.

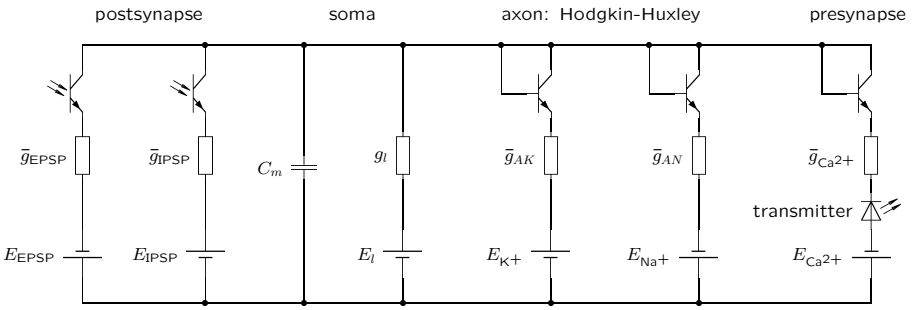

Fig. 1.21. Equivalent circuit for a neural point model

1.4.2 Compartment Models

Point models have one serious disadvantage: They completely disregard the spatial extension of the cell and the fact that different membrane patches, e.g. at the soma, the axon, the terminals, or the dendrites, exhibit different potentials (cf. Chap. 2). The gradients between these sites then lead to ion currents through the cell plasma thus contributing to the mechanisms of *spatial integration*. Moreover, currents moving back through the extracellular space give rise to the *somato-dendritic field potentials* (DFP). These fields sum to the local field potentials (LFP) at a mesoscopic and to electrocorticogram (ECoG) and electroencephalogram (EEG) at macroscopic scales [38–42] (cf. Chaps. 8 and 7 in this volume).

Correctly, the spatiotemporal dynamics of neuronal membranes must be treated by the *cable equation* [12, 13, 15, 18, 22, 24, 25]. This is a second-order partial differential equation for the membrane potential $U(\boldsymbol{r}, t)$. For the sake of numerical simulations, its discretized form leads to compartment models where individual membrane patches are described by the equivalent circuits discussed in the previous sections [12, 13, 15, 16, 18, 40, 41]. As an example, I shall create an equivalent circuit for a three-compartment model for the cortical pyramidal cells that is able to describe somato-dendritic field potentials.

Pyramidal cells are characterized by their axial symmetry. They consist of an *apical dendritic tree* comprising only excitatory synapses and a *basal dendritic tree* where mainly inhibitory synapses are situated. Both types of synapses are significantly separated in space thus forming a dipole of current sources (the inhibitory synapses) and sinks (the excitatory synapses) [38, 39, 41, 42]. The extracellular current flows from the sources to the sinks through a non-negligible resistance R_{out} which entails the somato-dendritic field. Therefore, we divide the pyramidal cell into three compartments: the first represents the apical dendrites, the second the basal dendrites, and the third takes firing into account. Figure 1.22 depicts its equivalent circuit. The internal resistance R_{int} accounts for the *length constant* of the neuron and contributes also to the synaptic weights (see Chap. 7).

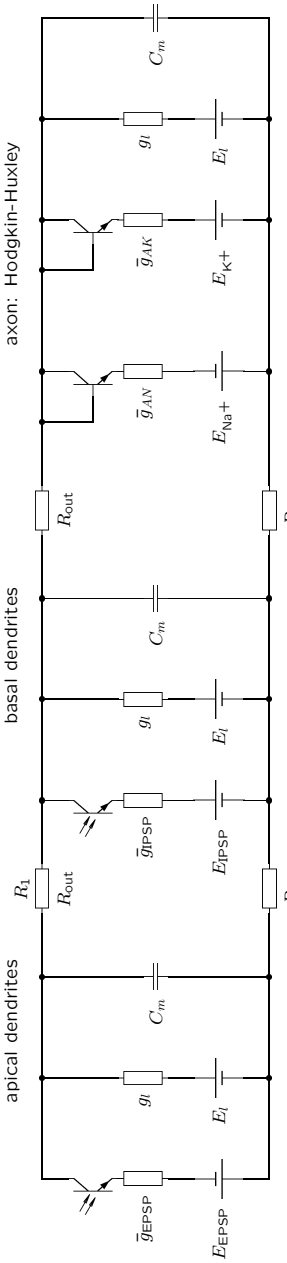

Fig. 1.22. Equivalent circuit for a three-compartment model of a pyramidal cell

In this model, the extracellular current I_{out} flowing from the inhibitory to the excitatory compartment through R_1 entails the dendritic field potential

$$U^{\text{DFP}} = \frac{I_{\text{out}}}{R_1} \,. \tag{1.64}$$

Note that I_{out} is large for a large difference between the EPSP and the IPSP, i.e. when both types of synapses are synchronously activated. In this case, however, the remaining current $I - I_{\text{out}}$ flowing through the axonal compartment can be too small to elicit action potentials. Therefore, DFP and spiking are inversely related with each other [41].

1.4.3 Reduced Models

The computational complexity of conductance models prevents numerical simulations of large neural networks. Therefore, simplifications and approximations have been devised and employed by several authors [10–18, 43–50].

In the following, we shall consider networks composed from n model neurons. Their membrane potentials U_i ($1 \leq i \leq n$) span the *observable state space*, such that $\boldsymbol{U} \in \mathbb{R}^n$; note that the proper phase space of the neural network might be of higher dimension. The observables U_i depend on the total postsynaptic current

$$I_i^{\text{PSC}} = -\sum_{j=1}^{n} w_{ij}\, I_j - I_i^{\text{ext}} \,, \tag{1.65}$$

where w_{ij} is the *synaptic weight* of the connection from unit j to unit i, dependent on the synaptic gain $\bar{g}_{ij}$ that evolves during learning, thus reflecting *synaptic plasticity* (see Chap. 2), and the intracellular resistances (see Chap. 7). The capacitance in (1.57) has been deliberately neglected and I_i^{ext} denotes the externally controlled input to neuron i.

The McCulloch-Pitts Model

The coarsest simplification by McCulloch and Pitts [16, 18, 51, 52] replaces the involved Hodgkin-Huxley system (1.25, 1.27–1.29) by a threshold device with only two states: $X_i \in \{0, 1\}$ where 0 denotes the inactivated, silent, and 1 denotes the activated, firing state. The dynamics of a network of n McCulloch-Pitts units is governed by the equations

$$X_i(t+1) = \Theta(I_i^{\text{PSC}} - \theta_i) \,, \tag{1.66}$$

where t is the discretized time, θ_i the activation threshold for unit i, and $I_i = X_i$ have been identified.

Integrate-and-fire Models

The next step to make threshold units biologically more plausible is by taking the passive membrane properties as described by (1.57) into account. This leads to the class of (leaky) integrate-and-fire models [12,13,15,16,18,46,50]:

$$\begin{aligned} \tau_i \frac{\mathrm{d}U_i}{\mathrm{d}t} + U_i &= I_i^{\mathrm{PSC}} \\ X_i(t_k) &= \Theta(U_i(t_k) - \theta_i) \\ U_i(t_k) &\leftarrow E\,. \end{aligned} \tag{1.67}$$

Here, $U_i(t)$ describes the membrane potential of unit i, X_i and θ_i model the action potentials and the firing thresholds as in (1.66), and t_k are the firing times where the membrane potential is reset to its resting value E (indicated by the arrow).

Rate Models

In Sects. 1.3.1 and 1.3.3, we saw that the principles of frequency modulation are exploited for neural en- and decoding — at least for regular spiking dynamics. Therefore, it seems to be appropriate to replace the exact time-course of a spike train by its frequency, *firing rate*, or firing probability [53,54]. The latter approach leads to the problem of determining the value

$$R_i(t) = \mathrm{Prob}(U_i(t) \geq \theta_i) = \int \mathrm{d}^{n-1}u \int_{\theta_i}^{\infty} \rho(\boldsymbol{u}, t)\, \mathrm{d}u_i\,, \tag{1.68}$$

where we have to regard the membrane potentials $\boldsymbol{U}(t)$ as a multivariate stochastic variable in the observable space with expectation values $\bar{U}_i(t)$ and probability density function $\rho(\boldsymbol{u}, t)$. The first integral in (1.68) provides the marginal distribution in the ith observable subspace. The stochasticity assumption is justified by our treatment of the presynaptic potential in Sect. 1.3.2. Because every action potential starts a Bernoulli process which describes how many vesicles are to be released, this element of stochasticity propagates along the synapse. As we have characterized the distribution of the number of released vesicles by (1.36), the postsynaptic currents are normally distributed about their voltage-dependent means $\bar{I}_i(\bar{\boldsymbol{U}})$,

$$I_i^{\mathrm{PSC}} = -\sum_j w_{ij}\, (\bar{I}_j(\bar{\boldsymbol{U}}(t)) + \eta_j(t))\,, \tag{1.69}$$

where $\eta_j(t)$ are independent normally distributed stochastic processes with

$$\begin{aligned} \langle \eta_j(t) \rangle &= 0 \\ \langle \eta_j(t), \eta_k(t') \rangle &= Q_{jk}\, \delta(t - t')\,. \end{aligned} \tag{1.70}$$

Therefore, (1.57) has to be read as a stochastic differential (Langevin) [30,31] equation

$$\frac{\mathrm{d}U_i}{\mathrm{d}t} = K_i(\boldsymbol{U}) - \sum_j \alpha_i w_{ij} \eta_j(t)) \,, \tag{1.71}$$

where

$$K_i(\boldsymbol{U}) = -\alpha_i U_i - \sum_j \alpha_i w_{ij} \bar{I}_j(\bar{\boldsymbol{U}}) \tag{1.72}$$

are the deterministic drifting forces and $\sum_j \alpha_i w_{ij} \eta_j$ are stochastic fluctuations, obeying

$$\left\langle \sum_j \alpha_i w_{ij} \eta_j(t), \sum_l \alpha_k w_{kl} \eta_l(t') \right\rangle = R_{ik} \delta(t - t') \,, \tag{1.73}$$

with

$$R_{ik} = \sum_{jl} \alpha_i w_{ij} \, \alpha_k w_{kl} \, Q_{jl} \,; \tag{1.74}$$

here, we substituted $\alpha_i = \tau_i^{-1}$.

The probability distribution density $\rho(\boldsymbol{u}, t)$ is then obtained by solving the Fokker-Planck equation [30,31] associated to (1.71),

$$\frac{\partial \rho}{\partial t} = \sum_i \frac{\partial}{\partial u_i} [K_i(\boldsymbol{u}) \rho] + \frac{1}{2} \sum_{ik} R_{ik} \frac{\partial^2 \rho}{\partial u_i \partial u_k} \,. \tag{1.75}$$

In order to solve (1.75), we assume that the currents $\bar{I}_j$ do not explicitly depend on the mean membrane potential, and that they change rather slowly in comparison to the density ρ (the "adiabatic ansatz"). Then, (1.75) is linear and hence solved by the Gaussians

$$\rho(u, t) = \frac{1}{\sqrt{2\pi \sigma_U^2(t)}} \, \exp\left[-\frac{(u - \bar{U}(t))^2}{2\sigma_U^2(t)} \right] \tag{1.76}$$

as its stationary marginal distributions, where $\bar{U}(t)$ and $\sigma_U^2(t)$ have to be determined from $\bar{I}(t)$ and R_{ik}. Integrating (1.68) with respect to (1.76) yields the spike rate

$$R_i = f(\bar{U}_i) = \frac{1}{2} \operatorname{erfc}\left(\frac{\theta_i - \bar{U}_i}{\sqrt{2}\sigma_U} \right) \,, \tag{1.77}$$

with "erfc" denoting the complementary error function. In such a way, the stochastic threshold dynamics are translated into the typical *sigmoidal activation functions* $f(x)$ employed in computational neuroscience [7–9,11–13,15, 16,18].

Gathering (1.67, 1.77), a leaky integrator model [46] is obtained as

$$\tau_i \frac{\mathrm{d}U_i}{\mathrm{d}t} + U_i = \sum_j w_{ij} \, f(U_j) \,. \tag{1.78}$$

An alternative derivation of (1.78) can be found in Chap. 7 by disregarding the postsynaptic impulse response functions $G(t,t')$. If these are taken into account, instead an integro-differential equation

$$\tau_i \frac{\mathrm{d}U_i}{\mathrm{d}t} + U_i = \sum_j w_{ij} \int_{-\infty}^{t} G(t-t') f(U_j(t'))\,\mathrm{d}t' \tag{1.79}$$

applies.

The Rinzel-Wilson Model

The models to be discussed next are approximations for the full Hodgkin-Huxley equations (1.25, 1.27–1.29). Following Rinzel, Wilson and Trappenberg [14,16], the Hodgkin-Huxley equations exhibit two separated time-scales: at the fast scale, the opening of the sodium channels characterized by $m(t)$ happens nearly instantaneously such that $m(t)$ can be replaced by its stationary value m_∞. On the other hand, the opening rate for the potassium channels n and the inactivation rate h for the sodium channels exhibit an almost linear relationship $h = 1 - n$. The corresponding substitutions then lead to a two-dimensional system for each neuron i.

$$\begin{aligned} I_i &= C_m \frac{\mathrm{d}U_i}{\mathrm{d}t} + n_i^4\, \bar{g}_{AK}(U_i - E_{\mathrm{K}^+}) + \\ &\quad + m_\infty^3 (1-n_i)\, \bar{g}_{AN}(U_i - E_{\mathrm{Na}^+}) + g_l(U_i - E_l) \\ \frac{\mathrm{d}n_i}{\mathrm{d}t} &= \alpha_n\,(1-n_i) - \beta_n\, n_i \end{aligned} \tag{1.80}$$

which was applied for the plot in Fig. 1.15.

The FitzHugh-Nagumo Model

The same observation as in above led FitzHugh and Nagumo to their approximation of the Hodgkin-Huxley equations [13, 14, 18, 43, 50]. Here, a general linear relation $h = a - b\,n$ is used in combination with a coordinate transformation and rescaling to arrive at the *Bonhoeffer-Van-der-Pol-*, or likewise, *FitzHugh-Nagumo equations*,

$$\begin{aligned} \frac{\mathrm{d}U_i}{\mathrm{d}t} &= U_i - \frac{1}{3}U_i^3 - W_i + I_i \\ \frac{\mathrm{d}W_i}{\mathrm{d}t} &= \phi(U_i + a - bW_i)\,, \end{aligned} \tag{1.81}$$

with parameters ϕ, a, b.

The Morris-Lecar Model

Originally, the *Morris-Lecar model* was devised to describe the spiking dynamics of potassium- and calcium-controlled muscle fibers [12–14,18,50]. After introducing dimensionless variables and rescaled parameters, they read

$$\frac{\mathrm{d}U_i}{\mathrm{d}t} = -m_\infty \bar{g}_{AC}(U_i - 1) - W_i\,\bar{g}_{AK}(U_i - E_{\mathrm{K}^+}) - g_l(U_i - E_l) + I_i \quad (1.82)$$

$$\frac{\mathrm{d}W_i}{\mathrm{d}t} = \alpha_W\,(1 - W_i) - \beta_W\,W_i\,.$$

The Morris-Lecar model has been extensively employed during the Summer School, see Chaps. 9, 11, 12, 14.

The Hindmarsh-Rose Model

The FitzHugh-Nagumo and Morris-Lecar models have the disadvantage that they do not have a bursting regime in their parameter space [50]. In order to overcome this obstacle, a third dimension for the phase space is necessary. The *Hindmarsh-Rose equations*, which exhibit this third dimension, are [14, 47]

$$\begin{aligned}\frac{\mathrm{d}U_i}{\mathrm{d}t} &= V_i - U_i^3 + 3U_i^2 + I_i - W_i \\ \frac{\mathrm{d}V_i}{\mathrm{d}t} &= 1 - 5U_i^2 - V_i \\ \frac{\mathrm{d}W_i}{\mathrm{d}t} &= r[s(U_i - U_0) - W_i]\,,\end{aligned} \quad (1.83)$$

with parameters r, s, U_0.

For applications of the Hindmarsh-Rose model in this book, see Chap. 6.

The Izhikevich Model

Making use of arguments from bifurcation theory, Izhikevich [49] approximated the Hodgkin-Huxley equations by the two-dimensional flow

$$\frac{\mathrm{d}U_i}{\mathrm{d}t} = 0.04U_i^2 + 5U_i + 140 - U_i + I_i \quad (1.84)$$

$$\frac{\mathrm{d}V_i}{\mathrm{d}t} = a(bV_i - U_i)\,, \quad (1.85)$$

disrupted by an auxiliary after-spike resetting

$$\text{if} \quad U_i \geq 30\,\mathrm{mV}, \quad \text{then} \begin{cases} U_i & \leftarrow & E \\ V_i & \leftarrow & V_i + c \end{cases}$$

with parameters a, b, c, E, where E denotes the resting potential.

A comprehensive comparison of different spiking neuron models with respect to their biological plausibility and computational complexity can be found in [50].

Also the Izhikevich model has been used during the Summer School. These results are presented in Chap. 13.

1.4.4 Neural Field Theories

For very large neural networks, a continuum approximation by spatial coarse-graining suggests itself [55–70]. Starting from the rate equation (1.79), the sum over the nodes connected with unit i has to be replaced by an integral transformation of a neural field quantity $U(x,t)$, where the continuous parameter x now indicates the position i in the network. Correspondingly, the synaptic weights w_{ij} turn into a kernel function $w(x,y)$. In addition, for large networks, the propagation velocity c of neural activation has to be taken into account. Therefore, (1.79) assumes the retarded form

$$\tau(x)\,\frac{\partial U(x,t)}{\partial t}+U(x,t)=\int_{-\infty}^{t}\mathrm{d}t'\int\mathrm{d}x' w(x,x')G(t-t')f\left[U\left(x',t'-\frac{|x-x'|}{c}\right)\right], \tag{1.86}$$

which can be transformed into a wave equation under additional assumptions. For further details, consult Chap. 8 and the references above.

1.5 Mass Potentials

Neural field theories [55–70] as well as population models of cortical modules [39, 71–81] (see also Chap. 7) describe mass potentials such as LFP or EEG as spatial sums of the EPSPs and IPSPs of cortical pyramidal cells. In these accounts, the somato-dendritic field potential (DFP) of an infinitesimally small volume element of cortical tissue, or of a single neuron, respectively, is described [79] by

$$U^{\mathrm{DFP}}=U^{\mathrm{EPSP}}+U^{\mathrm{IPSP}} \tag{1.87}$$

when $U^{\mathrm{EPSP}}>0, U^{\mathrm{IPSP}}<0$.[4] Unfortunately, this description is at variance with the physiological origin of the DFP. Looking at the equivalent circuit of the three-compartment model in Fig. 1.22, one easily recognizes that simultaneously active excitatory and inhibitory synapses give rise to a large voltage drop along the resistor R_1 separating both kind of synapses in space. Therefore, a large extracellular current yields a large DFP according to (1.64). On the other hand, the sum in (1.87) becomes comparatively small since EPSP and IPSP almost compensate each other. Therefore, the geometry and anatomy of pyramidal cells and cortex have to be taken into account. To this end, I shall mainly review the presentation of Nunez and Srinivasan [42, 82] in the following.

[4] The signs in (1.87) are physiologically plausible (cf. (1.43, 1.55)), whereas Jansen et al. [75, 76], Wendling et al. [77, 78], and David and Friston [79] assume that EPSP and IPSP both have positive signs such that their estimate for the DFP reads $U^{\mathrm{DFP}}=U^{\mathrm{EPSP}}-U^{\mathrm{IPSP}}$ (cf. Chap. 5).

1.5.1 Dendritic Field Potentials

If the reader takes a look at Fig. 8.1 in Chap. 8, she or he sees three triangular knobs that are the cell bodies of three pyramidal cells. Starting from their bases, axons proceed downwards like the roots of plants. In the other direction, they send strongly branched trees of dendrites towards the surface of the cortex. Pyramidal cells exhibit roughly an axonal symmetry and they are very densely packed in parallel, forming a fibrous tissue. Excitatory and inhibitory synapses are spatially separated along the dendritic tree: Excitatory synapses are mainly situated at the apical (i.e. the top-most) dendrites, while inhibitory synapses are arranged at the soma and the basal dendrites of the cells. This arrangement is functionally significant as the inhibitory synapses very effectively suppress the generation of action potentials by establishing short-cuts [41].

From the viewpoint of the extracellular space, inhibitory synapses act as current sources while excitatory synapses are current sinks. The extracellular space itself can be regarded as an electrolyte with (volume-) conductance $\sigma(\boldsymbol{x})$, where $\boldsymbol{x}$ indicates the dependence on the spatial position. From Maxwell's equations for the electromagnetic field, a continuity equation

$$-\nabla \cdot (\sigma \, \nabla \phi) + \frac{\partial \rho}{\partial t} = 0 \tag{1.88}$$

can be derived for the "wet-ware" [42, 82]. Here, $\phi(\boldsymbol{x})$ denotes the electric potential and $\rho(\boldsymbol{x}, t)$ the charge density, and $\boldsymbol{j} = -\sigma \, \nabla \phi$ is the current density according to Ohm's Law (1.5). Assuming that the conductivity $\sigma(\boldsymbol{x})$ is piecewise constant in the vicinity of a pyramidal cell, σ can be removed from the scope of the first gradient, yielding

$$-\sigma \Delta \phi + \frac{\partial \rho}{\partial t} = 0 \, . \tag{1.89}$$

Next, we have to describe the change of the current density. Setting

$$\frac{\partial \rho(\boldsymbol{x})}{\partial t} = \sum_i I_i \delta(\boldsymbol{x} - \boldsymbol{x_i}) \tag{1.90}$$

describes the postsynaptic transmembrane currents in the desired way as point sources and sinks located at $\boldsymbol{x_i}$. When we insert (1.90) into (1.89), we finally arrive at a Poisson equation

$$\sigma \Delta \phi = \sum_i I_i \delta(\boldsymbol{x} - \boldsymbol{x_i}) \tag{1.91}$$

in complete analogy to electrostatics.

Equation (1.91) can be easily solved by choosing appropriate boundary conditions that exclude the interiors and the membranes of the cells from the

domain of integration.[5] Integrating (1.91) over the extracellular space gives

$$\phi(\boldsymbol{x}) = \frac{1}{4\pi\sigma} \sum_i \frac{I_i}{r_i}\,, \tag{1.92}$$

where $\boldsymbol{x}$ denotes the observation site and $r_i = |\boldsymbol{x} - \boldsymbol{x_i}|$ abbreviates the distance between the point sources and sinks I_i and $\boldsymbol{x}$.

If the distance of the observation site $\boldsymbol{x}$ is large in comparison to the respective distances of the current sources and sinks from each other, the potential $\phi(\boldsymbol{x})$ can be approximated by the first few terms of a multipole expansion,

$$\phi(\boldsymbol{x}) = \frac{1}{4\pi\sigma} \left(\frac{1}{x} \sum_i I_i + \frac{1}{x^3} \sum_i I_i\, \boldsymbol{x}_i \cdot \boldsymbol{x} + \dots \right) . \tag{1.93}$$

Now, x denotes the distance of the observation point from the center of mass of the current cloud I_i. Due to the conservation of charge, the monopole term vanishes, whereas the higher order multipoles strongly decline with $x \to \infty$. Therefore, only the dipole term accounts for the DFP,

$$\phi^{\mathrm{DFP}}(\boldsymbol{x}) = \frac{1}{4\pi\sigma} \frac{1}{x^3} \sum_i I_i\, \boldsymbol{x}_i \cdot \boldsymbol{x} = \frac{1}{4\pi\sigma} \frac{\boldsymbol{p} \cdot \boldsymbol{x}}{x^3}\,, \tag{1.94}$$

where the dipole moment of the currents

$$\boldsymbol{p} = I(\boldsymbol{x}_1 - \boldsymbol{x}_2) = I\boldsymbol{d} \tag{1.95}$$

can be introduced when a current source $+I$ and a sink $-I$ are separated by the distance d. The unit vector $\boldsymbol{d}/d$ points from the source to the sink.

Equation (1.95) now suggests a solution for the problem with (1.87). The DFP is proportional to the dipole moment which depends monotonically on the absolute value I. Assuming that the excitatory and the inhibitory branch in the equivalent circuit in Fig. 1.22 are symmetric, the dipole moment, which is determined by I_{out}, depends on the difference between the (positive) EPSP and the (negative) IPSP,

$$U^{\mathrm{DFP}} = U^{\mathrm{EPSP}} - U^{\mathrm{IPSP}}\,, \tag{1.96}$$

such that a simple change of the sign corrects (1.87).

[5] My presentation here deviates from that given by Nunez and Srinivasan [42] who assume quasi-stationary currents $[\nabla \cdot \boldsymbol{j} = 0]$. As a consequence of (1.88), the change of the charge density would also vanish leading to a trivial solution. In order to circumvent this obstacle, Nunez and Srinivasan [42, p. 166] decompose the current into an "ohmic" part $-\sigma\nabla\phi$ and peculiar "impressed currents" $\boldsymbol{J}_S$ corresponding to EPSC and IPSC that cross the cell membranes. However, they concede that "the introduction of this pseudo-current may, at first, appear artificial and mysterious" aiming at the representation of the boundary conditions. This distinction is actually unnecessary when boundary conditions are appropriately chosen [82]. Nevertheless, Nunez' and Srinivasan's argument became very popular in the literature, e.g. in [4, 67].

1.5.2 Local Field potentials

Since pyramidal cells are aligned in parallel, they form a dipole layer of thickness d when they are synchronized within a cortical module. Subsequently, we will identify such modules with the anatomical columns (cf. Chap. 8) in order to compute the collective DFP, i.e. the local field potential (LFP) generated by a mass of approximately 10,000 pyramidal cells.

The current differential $\mathrm{d}I$ is then proportional to the infinitesimal area in cylindrical coordinates

$$\mathrm{d}I = j\mathrm{d}A\,, \tag{1.97}$$

where the current density j is assumed to be a constant scalar within one column. Hence, the differential of the potential $\mathrm{d}\phi$ at a distance z perpendicular to a cortical column of radius R that is contributed by the current $\mathrm{d}I$ is given by

$$\mathrm{d}\phi(\boldsymbol{x}) = \frac{1}{4\pi\sigma}\frac{j\,\boldsymbol{d}\cdot(\boldsymbol{x}-\boldsymbol{x}')}{|\boldsymbol{x}-\boldsymbol{x}'|^3}\mathrm{d}A\,, \tag{1.98}$$

where $\boldsymbol{x}'$ varies across the area of the module. Making use of the geometry depicted in Fig. 1.23 yields

$$\begin{aligned}
\mathrm{d}\phi(z) &= \frac{1}{4\pi\sigma}\frac{jd\sqrt{r^2+z^2}\cos\vartheta}{(r^2+z^2)^{3/2}}\,r\,\mathrm{d}r\,\mathrm{d}\varphi \\
&= \frac{jd}{4\pi\sigma}\frac{z\sqrt{r^2+z^2}}{\sqrt{r^2+z^2}(r^2+z^2)^{3/2}}\,r\,\mathrm{d}r\,\mathrm{d}\varphi \\
&= \frac{jd}{4\pi\sigma}\frac{rz}{(r^2+z^2)^{3/2}}\,\mathrm{d}r\mathrm{d}\varphi \\
\phi(z) &= \frac{jd}{4\pi\sigma}\int_0^{2\pi}\mathrm{d}\varphi\int_0^{R}\mathrm{d}r\;\frac{rz}{(r^2+z^2)^{3/2}}\,.
\end{aligned}$$

Performing the integration then gives the LFP perpendicular to the dipole layer

$$\phi^{\mathrm{LFP}}(z) = \frac{jd}{2\sigma}\left(1-\frac{z}{\sqrt{R^2+z^2}}\right)\,. \tag{1.99}$$

1.5.3 Electroencephalograms

Equation (1.99) describes the summed potential resulting from the synchronized synaptic activity of all pyramidal neurons in a column in a distance z above the cortical gray matter. By integrating over a larger domain of cortical tissue, e.g. over a macrocolumn, one obtains an estimator of the electrocorticogram (ECoG) [83]. In order to compute the electroencephalogram (EEG), one has to take the different conductances of skull and scalp into account. Nunez and Srinivasan [42] discuss different scenarios with different

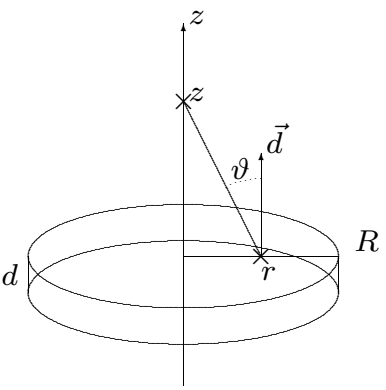

Fig. 1.23. Geometry of a cortical column

geometries. In the simplest case, only one interface between a conductor (G_1) with conductance σ_1 and an isolator G_2 (conductance $\sigma_2 = 0$) is considered. According to the respective interpretation, either the skull, or the air above the subject's head is regarded to be the isolator.[6]

In one case, one has to consider the potential generated by a point source (or sink) I at a distance $-h$ from the interface in the semi-space G_1 by attaching a mirror source (or sink) I' at a distance h from the interface in order to solve Dirichlet's boundary problem if $\boldsymbol{x} \in G_2, z > 0$ [42]. In the other case, one has to replace the source (or sink) I in the semi-space G_1 by another source (or sink) $I + I''$ if $\boldsymbol{x} \in G_1, z < 0$. The geometrical situation is shown in Fig. 1.24.

In the semi-space G_2 relevant for the EEG measurement, (1.91) is then solved by

$$\phi^{\mathrm{DFP}}(\boldsymbol{x}) = \frac{1}{2\pi(\sigma_1 + \sigma_2)} \frac{I}{\sqrt{r^2 + (z+h)^2}} \,. \tag{1.100}$$

When G_2 is assumed to be an isolator, we set $\sigma_2 = 0$, $\sigma_1 \equiv \sigma$. Hence the potential in the semi-space G_2 is simply twice the potential in a homogeneous medium. Provided that all current sources and sinks are distributed in G_1, the superposition principle entails

$$\phi^{\mathrm{DFP}}(\boldsymbol{x}) = \frac{1}{2\pi\sigma} \sum_i \frac{I_i}{\sqrt{r_i^2 + (z+h_i)^2}} \,. \tag{1.101}$$

From (1.99) follows

[6] Occasionally a misunderstanding occurs in the literature where ionic currents and dielectric displacement, i.e. polarization, are confused [84, 85]. Do we really measure sodium or potassium ions that have traversed the skull during an EEG measurement, or is the skull merely a polarizable medium?

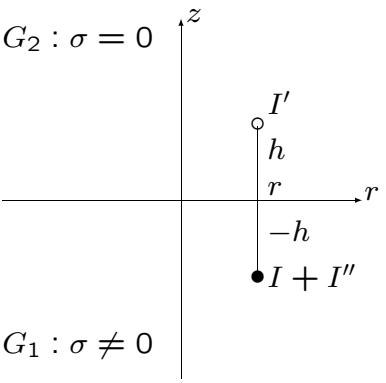

Fig. 1.24. Geometry of Dirichlet's boundary problem for the EEG

$$\Phi(z) \equiv \phi^{\mathrm{EEG}} = \frac{jd}{\sigma}\left(1 - \frac{z}{\sqrt{R^2 + z^2}}\right) \tag{1.102}$$

for the EEG generated by a cortical column measurable at the scalp.

1.5.4 Mean Fields

In this last subsection, I shall discuss the question of whether mass potentials such as LFP or EEG are mere epiphenomena [42,86], or whether they play a functional role in the organization of brain functioning. If the latter were the case, they would be described as *order parameters* which couple as *mean fields* onto the microscopic neurodynamics with the ability to enslave its behavior [30,87].

In order to encounter this problem, one has to estimate the average field strengths and voltage differences that are generated by synchronized activity of all pyramidal cells of a cortical module. These quantities then have to be compared with experimental findings on the susceptibility of nerve cells through electromagnetic fields. As mentioned above, the spiking threshold is around $\theta = -50\,\mathrm{mV}$, i.e. the membrane must be polarized by $\Delta U = 10\,\mathrm{mV} - 20\,\mathrm{mV}$ from its resting value given by the Nernst equation (1.7). This corresponds to an electric field strength $E = 10^6\,\mathrm{V/m}$ for a thickness of 5 nm of the cell membrane [88].

On the other hand, neurophysiological experiments have revealed that much smaller field strengths of about 1 V/m entail significant changes of neural excitability [89–93]. Event-related potentials can be modulated by values around 4 V/m. In the hippocampus, where pyramidal cells are very densely packed, effective field strengths are in the range of 5–7 V/m, whereas 10–15 V/m are needed in the cerebellum [91].

To estimate the field strength generated by a cortical column, we have to solve the Dirichlet boundary problem within the electrolyte G_1 as shown in

Fig. 1.24. The potential of a point source (or sink) I at $\boldsymbol{x} \cong (0,0,z)$ is given in the semi-space G_1 as

$$\phi(\boldsymbol{x}) = \frac{I}{4\pi\sigma_1}\left(\frac{1}{\sqrt{r^2+(z+h)^2}} + \frac{\sigma_1-\sigma_2}{\sigma_1+\sigma_2}\frac{1}{\sqrt{r^2+(z-h)^2}}\right). \tag{1.103}$$

Since we assume G_2 to be an isolator again ($\sigma_2 = 0$), the superposition principle yields

$$\phi(\boldsymbol{x}) = \frac{1}{4\pi\sigma}\sum_i I_i\left(\frac{1}{\sqrt{r_i^2+(z+h_i)^2}} + \frac{1}{\sqrt{r_i^2+(z-h_i)^2}}\right). \tag{1.104}$$

Next, we apply (1.104) to a current dipole made up by a source (or sink) I at $(r,\varphi,l-d/2)$ and a sink (or source) $-I$ at $(r,\varphi,l+d/2)$, where the dipole's center is situated in a distance l below the interface:

$$\phi(\boldsymbol{x}) = \frac{I}{4\pi\sigma}\left(\frac{1}{\sqrt{r^2+(z+l-d/2)^2}} + \frac{1}{\sqrt{r^2+(z-l+d/2)^2}} - \frac{1}{\sqrt{r^2+(z+l+d/2)^2}} + \frac{1}{\sqrt{r^2+(z-l-d/2)^2}}\right).$$

Approximating the quotients by $(1+x)^{-1/2} \approx 1 - x/2$ gives

$$\phi(\boldsymbol{x}) = \frac{Ild}{2\pi\sigma r^3}, \tag{1.105}$$

i.e. the potential depends only on the radial direction in the conductor. Therefore, the field strength is given by the r-component of the gradient

$$E = -\frac{\partial}{\partial r}\phi(\boldsymbol{x}) = \frac{3Ild}{2\pi\sigma r^4}. \tag{1.106}$$

In order to replace the column by an equivalent current dipole moment generating the same field, we have to compute the current density through the surface of the column according to (1.102) from the measured scalp EEG. Rearrangement of (1.102) yields

$$j = \frac{\sigma}{d}\,\frac{\Phi(z)}{1-\frac{z}{\sqrt{R^2+z^2}}}. \tag{1.107}$$

Then, the current through the column would be

$$I = j\pi R^2 \tag{1.108}$$

if the tissue were a continuum as presupposed in Sect. 1.5.2. Here, $R \approx 150\,\mu$m is the radius of a column. By contrast, one has to take into account that a

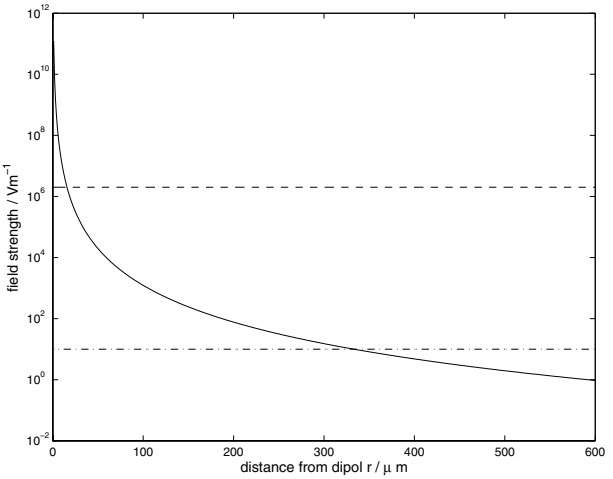

Fig. 1.25. Electric field strength estimated from the EEG depending on the distance of an equivalent dipole. The horizontal lines indicate critical field strengths for evoking action potentials (*upper line*), and for detectable physiological impact (*bottom line*)

column contains about 10,000 pyramidal cells. Thus, the current along a single pyramidal cell is

$$I_{\mathrm{Pyr}} = \frac{j\pi R^2}{N} \tag{1.109}$$

with $N = 10,000$. Inserting (1.109) and (1.107) into (1.106) gives with $z = l$

$$E(r) = \frac{3lR^2}{2Nr^4} \frac{\Phi(l)}{1 - \frac{l}{\sqrt{R^2+l^2}}} . \tag{1.110}$$

Figure 1.25 presents a plot of $E(r)$ for the parameter values $R = 150\,\mu\mathrm{m}$, $N = 10,000$, where a distance between the cortex surface and the skull $l = 8\,\mathrm{mm}$ and a peak EEG amplitude of $\Phi(l) = 100\,\mu\mathrm{V}$ have been assumed.

Additionally, Fig. 1.25 displays two lines: the upper line reflects the spiking threshold of a single neuron, $E = 10^6\,\mathrm{V/m}$; the bottom one indicates the limit of physiological efficacy, $E = 10\,\mathrm{V/m}$ [91]. These thresholds correspond to the distances $r_1 = 16.39\,\mu\mathrm{m}$, and $r_2 = 346.77\,\mu\mathrm{m}$ from the equivalent dipole. Because we took $R = 150\,\mu\mathrm{m}$ as the radius of a cortical module, r_2 reaches far into the neighboring column. With 10,000 pyramidal cells per module, their average distance amounts to $3\,\mu\mathrm{m}$, such that approximately 120 closely packed pyramidal cells can be excited by the mass potential. Interestingly, the radius r_2 coincides nicely with the size of the column. Hence, this rough estimate suggests that cortical columns are functional modules controlled by their own electric mean fields that are very likely not mere epiphenomena.

This is consistent with empirical findings. Adey [89] reported a change of the calcium conductivity of neuron membranes under the impact of sustained

high-frequency fields. In the hippocampus of rats, field effects are particularly pronounced due to the extreme packing density of the pyramidal cells and the resulting low conductivity of the extracellular liquid. Suppressing synaptic transmission experimentally by reducing the amount of available extracellular calcium, leads to the emergence of spontaneous *bursting* that can be synchronized by mass potentials [91]. Bracci et al. [90] demonstrated that the synchronization of hippocampal neurons is facilitated by the application of external electric fields. They showed also that the conductance of the extracellular electrolyte is a control parameter which can be tuned in such a way that spontaneous synchronization takes place if the conductance is lowered below a critical value. In this case, the fall of the dendritic field potentials along the extracellular resistors contribute to larger LFP and EEG that in turn enslave the whole population. Most recently, Richardson, Schiff and Gluckman [92, 93] studied the propagation of traveling waves through an excitable neural medium under the influence of external fields. They reported a dependence of the group velocity on the polarity of the applied field, and modeled these effects through a neural field theory analogue of (1.86).

Coming back to our neuron models, the impact of mass potentials can be formally taken into account by introducing a *mean field* coupling. Concerning, for example, the Hodgkin-Huxley equations (1.25, 1.27–1.29), one has to replace the membrane potential U_i of neuron i by a shifted value

$$U_i' = U_i - \sum_j U_j^{\mathrm{DFP}} \,, \tag{1.111}$$

where either the dendritic field potential is given by (1.64), or, in a continuum account, the whole sum is provided by (1.99). This idea has been expressed by Braitenberg and Schüz [94, p. 198], in that a cortical module controls its own activation thresholds.

1.6 Discussion

In this chapter, I have sketched the basic principles of neurophysics, i.e. the biophysics of membranes, neurons, neural networks and neural masses. Let me finally make some concluding remarks on neural modeling and descriptions. I hope the reader has recognized that there is no unique *physical model* of *the* neuron, or of *the* neural network of the brain. Even a single neuron can be described by models from different complexity classes. It can be regarded as a continuous system governed by a nonlinear partial differential equation which describes its cable properties. Decomposing the cable into compartments, one obtains either compartment models comprised of lots of coupled ordinary differential equations, or point models that are still described by many coupled ordinary differential equations, one for the kinetics of each population of ion channels. Further simplifying these models, one eventually arrives at the coarsest McCulloch-Pitts neuron [51].

On the other hand, each neuron model dictates the dimensionality of its phase space and, as its projection, its observable space. Observables provide the interface to experimental neuroscience in that they should be *observable*. The best theoretical neuron model is not much good if it contains quantities that are not observable in real experiments. In most cases, observables are membrane potentials either collected from the axons, i.e. action potentials, or measured from the dendro-somatic membranes such as EPSP and IPSP. However, a few electrode tips put into a couple of neurons will not provide sufficiently many observables for describing the behavior of a neural network. At the network level, the abovementioned problems greatly worsen with increasing size and complexity of the network, ending in an unmanageable number of degrees of freedom for continuum models.

In this case, spatial coarse-graining [62] is the method of choice. By averaging activity across regions of appropriate size, one obtains mass potentials such as LFP or EEG. LFP is experimentally observable through the use of multi-electrode arrays placed into the extracellular space. Each sensor collects averaged dendritic field potentials from several thousands of neurons, as well as some spiking activity in its vicinity. On the other hand, ECoG (intracranial EEG) and EEG are gathered by electrodes placed at the cerebral membrane or at the scalp, respectively. Each electrode registers the mean activity of billions of neurons. Using conventional 32, 64, or 128 channel amplifiers thereby collapses the huge microscopic observable space of single neurons and the large mesoscopic observable space of LFP to a macroscopic observable space of 32, 64, or 128 dimensions.

As we have seen in Sect. 1.5.3, such mass potentials are not in the least irrelevant because they serve as order parameters [30,87], both indicating and causing macroscopic ordering of the system. Yet there is another important aspect of mass potentials. They do not only comprise a spatial coarse-graining by definition, but also provide a coarse-graining of the high-dimensional microscopic phase space. Consider a mean field observable

$$F(x) = \sum_i f_i(\boldsymbol{x})\,, \tag{1.112}$$

where the sum extends over a population of n neurons and f_i denotes a projection of the microscopic state $\boldsymbol{x} \in X$ onto the i-th coordinate axis measuring the activation $f_i(\boldsymbol{x}) = x_i$ of the ith neuron. Obviously, the outcomes of F may have multiple realizations as the terms in the sum in (1.111) can be arbitrarily arranged. Therefore, two neural activation vectors $\boldsymbol{x}, \boldsymbol{y}$ can lead to the same value $F(\boldsymbol{x}) = F(\boldsymbol{y})$ (e.g. when $f_i(\boldsymbol{x}) - \epsilon = f_j(\boldsymbol{x}) + \epsilon$, $i \neq j$), so that they are indistinguishable by means of F. Beim Graben and Atmanspacher [95] call such microstates *epistemically equivalent*. All microstates that are epistemically equivalent to each other form an equivalence class, and, as it is well known from set theory, all equivalence classes partition the phase space X. If the equivalence classes of F in X form a finite partition $\mathcal{Q} = \{A_1, \ldots A_I\}$ of X, one can assign symbols a_i from an alphabet $\mathbf{A}$ to the cells A_i and obtain

a *symbolic dynamics* [96–98]. In this way, experimentally well-defined meso- and macroscopic brain observables, LFP and EEG, form a coarse-grained description of the underlying microscopic neurodynamics.

Atmanspacher and beim Graben [99,100] discuss this coarse-graining with respect to its stability properties. The microscopic dynamics $\boldsymbol{x} \mapsto \Phi^t(\boldsymbol{x})$ where the *flow* Φ solves the microscopic differential equations, is captured by transitions from one symbol to another one $a_i \mapsto a_j$. If these transitions can be described by an ergodic Markov chain, the symbolic dynamics exhibits particular stability properties. If the Markov chain is aperiodic, a distinguished thermal equilibrium state can be constructed for the symbolic description. If, contrarily, the Markov chain is periodic, the system possesses stable fixed point or limit cycle attractors. Atmanspacher and beim Graben argue that in both cases, the concept of *contextual emergence* applies where higher-level descriptions emerge from contingently supplied contexts that are not merely reducible to lower-level descriptions. As an application, Atmanspacher and beim Graben [99, 100] demonstrated the contextual emergence of neural correlates of consciousness [101] from neurodynamics where arbitrary contexts are given by phenomenal families partitioning the space of phenomenal experiences [102]. Other examples were discussed by beim Graben [103] and Dale and Spivey [104] where symbolic cognition emerges from partitioned dynamical systems.

The problem of finding reasonable macroscopic observables for neural networks has been addressed by Amari [52]. He considered random networks of McCulloch-Pitts neurons (cf. Chaps. 3, 5, 7), and defined a proper macrostate as a macroscopic observable such as (1.112) if two conditions hold: Firstly, the temporal evolution of the observable should be compatible with the coarse-graining, and, secondly, the observable should be structurally stable against topological deformations of the network. The second requirement is closely related to ergodicity of the resulting symbolic dynamics [99]. Accordingly, the first demand entails that all initial conditions that are mapped onto the same value of a macrostate are epistemically equivalent. As an example for a good macrostate, at least for his toy-model, Amari [52] provided the mass potential (1.112). Hence, macroscopic descriptions of neural masses provide important insights into the functional organization of neurodynamical systems. They are by far more then mere epiphenomena.

Acknowledgements

This chapter is based on notes from a lecture course “Introduction to Neurophysics”, I taught together with J. Kurths, D. Saddy, and T. Liebscher in the years 2000 and 2002 at the University of Potsdam for the DFG Research Group “Conflicting Rules in Cognitive Systems”. Section 1.5 contains parts of my thesis [82] that were previously available only in German. Section 1.6 presents some results from a cooperation with H. Atmanspacher. S. J. Nasuto,

J. J. Wright and C. Zhou helped me improving this chapter. I greatly acknowledge their respective contributions and inspiring discussions.

References

1. J. von Neumann. *The Computer and the Brain*. Yale University Press, New Haven (CT), 1958. Partly reprinted in J. A. Anderson and E. Rosenfeld (1988), p. 83ff.
2. Z. W. Pylyshyn. *Computation and Cognition: Toward a Foundation for Cognitive Science*. MIT Press, Cambrigde (MA), 1986.
3. J. R. Anderson. *Cognitive Psychology and its Implications*. W. H. Freeman and Company, New York (NY), 4th edition, 1995.
4. M. Kutas and A. Dale. Electrical and magnetic readings of mental functions. In M. Rugg, editor, *Cognitive Neuroscience*, pp. 197–242. Psychology Press, Hove East Sussex, 1997.
5. R. C. O'Reilly and Y. Munakata. *Computational Explorations in Cognitive Neuroscience. Understanding the Mind by Simulating the Brain*. MIT Press, Cambridge (MA), 2000.
6. M. S. Gazzaniga, R. B. Ivry, and G. R. Mangun, editors. *Cognitive Neuroscience. The Biology of the Mind*. W. W. Norton, New York (NY), 2nd edition, 2002.
7. J. A. Anderson and E. Rosenfeld, editors. *Neurocomputing. Foundations of Research*, Vol. 1. MIT Press, Cambridge (MA), 1988.
8. J. A. Anderson, A. Pellionisz, and E. Rosenfeld, editors. *Neurocomputing. Directions for Research*, Vol. 2. MIT Press, Cambridge (MA), 1990.
9. P. S. Churchland and T. J. Sejnowski. *The Computational Brain*. MIT Press, Cambridge (MA), 1994.
10. F. Riecke, D. Warland, R. de Ruyter van Steveninck, and W. Bialek. *Spikes: Exploring the Neural Code*. Computational Neurosciences. MIT Press, Cambridge (MA), 1997.
11. M. A. Arbib, editor. *The Handbook of Brain Theory and Neural Networks*. MIT Press, Cambridge (MA), 1998.
12. C. Koch and I. Segev, editors. *Methods in Neuronal Modelling. From Ions to Networks*. Computational Neuroscience. MIT Press, Cambridge (MA), 1998.
13. C. Koch. *Biophysics of Computation. Information Processing in Single Neurons*. Computational Neuroscience. Oxford University Press, New York (NY), 1999.
14. H. R. Wilson. *Spikes, Decisions and Actions. Dynamical Foundations of Neuroscience*. Oxford University Press, New York (NY), 1999.
15. P. Dayan and L. F. Abbott. *Theoretical Neuroscience*. Computational Neuroscience. MIT Press, Cambridge (MA), 2001.
16. T. P. Trappenberg. *Fundamentals of Computational Neuroscience*. Oxford University Press, Oxford (GB), 2002.
17. R. P. N. Rao, B. A. Olshausen, and M. S. Lewicky, editors. *Probabilistic Models of the Brain: Perception and Neural Function*. MIT Press, Cambridge (MA), 2002.
18. W. Gerstner and W. Kistler. *Spiking Neuron Models. Single Neurons, Populations, Plasticity*. Cambridge University Press, Cambridge (UK), 2002.

19. E. R. Kandel, J. H. Schwartz, and T. M. Jessel, editors. *Principles of Neural Science*. Appleton & Lange, East Norwalk, Connecticut, 1991.
20. E. R. Kandel, J. H. Schwartz, and T. M. Jessel, editors. *Essentials of Neural Science and Behavior*. Appleton & Lange, East Norwalk, Connecticut, 1995.
21. J. G. Nicholls, A. R-Martin, B. G. Wallace, and P. A. Fuchs. *From Neuron to Brain*. Sinauer, Sunderland (MA), 2001.
22. H. C. Tuckwell. *Introduction to Theoretical Neurobiology*, Vol. 1. Cambridge University Press, Cambridge (UK), 1988.
23. H. C. Tuckwell. *Introduction to Theoretical Neurobiology*, Vol. 2. Cambridge University Press, Cambridge (UK), 1988.
24. D. Johnston and S. M.-S. Wu. *Foundations of Cellular Neurophysiology*. MIT Press, Cambridge (MA), 1997.
25. B. Hille. *Ion Channels of Excitable Membranes*. Sinauer, Sunderland, 2001.
26. A. Einstein. Eine neue Bestimmung der Moleküldimensionen. *Annalen der Physik*, 19:289–306, 1906.
27. S. B. Laughlin, R. R. de Ruyter van Steveninck, and J. C. Anderson. The metabolic cost of neural information. *Nature Neuroscience*, 1(1): 36–41, 1998.
28. W. W. Orrison Jr., J. D. Lewine, J. A. Sanders, and M. F. Hartshorne. *Functional Brain Imaging*. Mosby, St. Louis, 1995.
29. N. K. Logothetis, J. Pauls, M. Augath, T. Trinath, and A. Oeltermann. Neurophysiological investigation of the basis of the fMRI signal. *Nature*, 412: 150–157, 2001.
30. H. Haken. *Synergetics. An Introduction*, Vol. 1 of *Springer Series in Synergetics*. Springer, Berlin, 1983.
31. N. G. van Kampen. *Stochastic Processes in Physics and Chemistry*. Elsevier, Amsterdam, 1992.
32. A. L. Hodgkin and A. F. Huxley. A quantitative description of membrane current and its application to conduction and excitation in nerve. *J. Physiol.*, 117: 500–544, 1952.
33. I. Swameye, T. G. Müller, J. Timmer, O. Sandra, and U. Klingmüller. Identification of nucleocytoplasmatic cycling as a remote sensor in cellular signaling by databased modeling. *Proceedings of the National Academy of Sciences of the U.S.A.*, 100(3): 1028–1033, 2003.
34. J. M. Bower and D. Beeman. *The Book of `GENESIS`. Exploring Realistic Neural Models with the GEneral NEural SImulation System*. Springer, New York (NY), 1998.
35. J. W. Moore and M. L Hines. *Simulations with `NEURON`*. Duke and Yale University, 1994.
36. A. Destexhe, D. Contreras, and M. Steriade. Cortically-induced coherence of a thalamic-generated oscillation. *Neuroscience*, 92(2): 427–443, 1999.
37. C. Bédard, H. Kröger, and A. Destexhe. Modeling extracellular field potentials and the frequency-filtering properties of extracellular space. *Biophys. J.*, 86(3): 1829–1842, 2004.
38. O. Creutzfeld and J. Houchin. Neuronal basis of EEG-waves. In *Handbook of Electroencephalography and Clinical Neurophysiology*, Vol. 2, Part C, pp. 2C-5–2C-55. Elsevier, Amsterdam, 1974.
39. W. J. Freeman. *Mass Action in the Nervous System*. Academic Press, New York (NY), 1975.

40. D. T. J. Liley, D. M. Alexander, J. J. Wright, and M. D. Aldous. Alpha rhythm emerges from large-scale networks of realistically coupled multicompartmental model cortical neurons. *Network: Comput. Neural Syst.*, 10: 79–92, 1999.
41. A. J. Trevelyan and O. Watkinson. Does inhibition balance excitation in neocortex? *Prog. Biophys. Mol. Biol.*,, 87: 109–143, 2005.
42. P. L. Nunez and R. Srinivasan. *Electric Fields of the Brain: The Neurophysics of EEG*. Oxford University Press, New York, 2006.
43. R. FitzHugh. Impulses and physiological states in theoretical models of nerve membrane. *Biophys. J.*, 1: 445–466, 1961.
44. T. Pavlidis. A new model for simple neural nets and its application in the design of a neural oscillator. *Bull. Math. Biol.*, 27: 215–229, 1965.
45. R. B. Stein, K. V. Leung, M. N. Oğuztöreli, and D. W. Williams. Properties of small neural networks. *Kybernetik*, 14:223–230, 1974.
46. R. B. Stein, K. V. Leung, D. Mangeron, and M. N. Oğuztöreli. Improved neuronal models for studying neural networks. *Kybernetik*, 15: 1–9, 1974.
47. J. L. Hindmarsh and R. M. Rose. A model of neuronal bursting using three coupled first-order differential equations. *Proceedings of the Royal Society London*, B221:87–102, 1984.
48. N. F. Rulkov. Modeling of spiking-bursting neural behavior using two-dimensional map. *Phys. Rev. E*, 65: 041922, 2002.
49. E. M. Izhikevich. Simple model of spiking neurons. *IEEE Trans. Neural Networks*, 14(6): 1569–1572, 2003.
50. E. M. Izhikevich. Which model to use for cortical spiking neurons? *IEEE Trans. Neural Networks*, 15(5): 1063–1070, 2004.
51. W. S. McCulloch and W. Pitts. A logical calculus of ideas immanent in nervous activity. *Bull. Math. Biophys.*, 5:115–133, 1943. Reprinted in J. A. Anderson and E. Rosenfeld (1988) [7], p. 83ff.
52. S. Amari. A method of statistical neurodynamics. *Kybernetik*, 14: 201–215, 1974.
53. D. J. Amit. *Modeling Brain Function. The World of Attractor Neural Networks*. Cambridge University Press, Cambridge (MA), 1989.
54. A. Kuhn, A. Aertsen, and S. Rotter. Neuronal integration of synaptic input in the fluctuation-driven regime. *J. Neurosci.*, 24(10): 2345–2356, 2004.
55. J. S. Griffith. A field theory of neural nets: I. derivation of field equations. *Bull. Math. Biophys.*, 25:111–120, 1963.
56. J. S. Griffith. A field theory of neural nets: II. properties of the field equations. *Bull. Math. Biophys.*, 27: 187–195, 1965.
57. H. R. Wilson and J. D. Cowan. A mathematical theory of the functional dynamics of cortical and thalamic nervous tissue. *Kybernetik*, 13: 55–80, 1973.
58. P. L. Nunez, editor. *Neocortical Dynamics and Human EEG Rhythms*. Oxford University Press, New York (NY), 1995.
59. V. K. Jirsa and H. Haken. Field theory of electromagnetic brain activity. *Phys. Rev. Lett.*, 77(5): 960–963, 1996.
60. V. K. Jirsa and H. Haken. A derivation of a macroscopic field theory of the brain from the quasi-microscopic neural dynamics. *Physica D*, 99: 503–526, 1997.
61. J. J. Wright and D. T. J. Liley. Dynamics of the brain at global and microscopic scales: Neural networks and the EEG. *Behavioral and Brain Sciences*, 19: 285–320, 1996.

62. D. T. J. Liley, P. J. Cadusch, and J. J. Wright. A continuum theory of electrocortical activity. *Neurocomputing*, 26–27: 795–800, 1999.
63. P. A. Robinson, C. J. Rennie, J. J. Wright, H. Bahramali, E. Gordon, and D. L. Rowe. Prediction of electroencephalic spectra from neurophysiology. *Phys. Rev. E*, 63, 2001. 021903.
64. C. J. Rennie, P. A. Robinson, and J. J. Wright. Effects of local feedback on dispersion of electrical waves in the cerebral cortex. *Phys. Rev. E.*, 59(3): 3320–3329, 1999.
65. P. A. Robinson, C. J. Rennie, J. J. Wright, and P. D. Bourke. Steady states and global dynamics of electrical activity in the cerebral cortex. *Phys. Rev. E.*, 58(3): 3557–3571, 1998.
66. J. J. Wright, C. J. Rennie, G. J. Lees, P. A. Robinson, P. D. Bourke, C. L. Chapman, E. Gordon, and D. L. Rowe. Simulated electrocortical activity at microscopic, mesoscopic, and global scales. *Neuropsychopharmacology*, 28: S80–S93, 2003.
67. V. K. Jirsa. Information processing in brain and behavior displayed in large-scale scalp topographies such as EEG and MEG. *Int. J. Bifurcation and Chaos*, 14(2): 679–692, 2004.
68. J. J. Wright, C. J. Rennie, G. J. Lees, P. A. Robinson, P. D. Bourke, C. L. Chapman, E. Gordon, and D. L. Rowe. Simulated electrocortical activity at microscopic, mesoscopic and global scales. *Int. J. Bifurcation and Chaos*, 14(2): 853–872, 2004.
69. J. J. Wright, P. A. Robinson, C. J. Rennie, E. Gordon, P. D. Burke, C. L. Chapman, N. Hawthorn, G. J. Lees, and D. Alexander. Toward an integrated continuum model of cerebral dynamics: the cerebral rhythms, synchronous oscillation and cortical stability. *Biosystems*, 63: 71–88, 2001.
70. V. K. Jirsa and J. A. S. Kelso. Spatiotemporal pattern formation in neural systems with heterogeneous connection toplogies. *Phys. Rev. E.*, 62(6): 8462–8465, 2000.
71. H. R. Wilson and J. D. Cowan. Excitatory and inhibitory interactions in localized populations of model neurons. *Biophys. J.*, 12: 1–24, 1972.
72. F. H. Lopes da Silva, A. Hoecks, H. Smits, and L. H. Zetterberg. Model of brain rhythmic activity: The alpha-rhythm of the thalamus. *Kybernetik*, 15: 27–37, 1974.
73. F. H. Lopes da Silva, A. van Rotterdam, P. Bartels, E. van Heusden, and W. Burr. Models of neuronal populations: The basic mechanisms of rhythmicity. In M. A. Corner and D. F. Swaab, editors, *Perspectives of Brain Research*, Vol. 45 of *Prog. Brain Res.*, pp. 281–308. 1976.
74. W. J. Freeman. Simulation of chaotic EEG patterns with a dynamic model of the olfactory system. *Biol. Cybern.*, 56: 139–150, 1987.
75. B. H. Jansen, G. Zouridakis, and M. E. Brandt. A neurophysiologically-based mathematical model of flash visual evoked potentials. *Biol. Cybern.*, 68: 275–283, 1993.
76. B. H. Jansen and V. G. Rit. Electroencephalogram and visual evoked potential generation in a mathematical model of coupled cortical columns. *Biol. Cybern.*, 73: 357–366, 1995.
77. F. Wendling, J. J. Bellanger, F. Bartolomei, and P. Chauvel. Relevance of nonlinear lumped-parameter models in the analysis of depth-EEG epileptic signals. *Biol. Cybern.*, 83: 367–378, 2000.

78. F. Wendling, F. Bartolomei, J. J. Bellanger, and P. Chauvel. Epileptic fast activity can be explained by a model of impaired GABAergic dendritic inhibition. *Eur. J. Neurosci.*, 15: 1499–1508, 2002.
79. O. David and K. J. Friston. A neural mass model for MEG/EEG: coupling and neuronal dynamics. *Neuroimage*, 20: 1743–1755, 2003.
80. O. David, D. Cosmelli, and K. J. Friston. Evaluation of different measures of functional connectivity using a neural mass model. *Neuroimage*, 21: 659–673, 2004.
81. O. David, L. Harrison, and K. J. Friston. Modelling event-related respones in the brain. *Neuroimage*, 25: 756–770, 2005.
82. P. beim Graben. *Symbolische Dynamik Ereigniskorrelierter Potentiale in der Sprachverarbeitung*. Berichte aus der Biophysik. Shaker Verlag, Aachen, 2001.
83. C. Baumgartner. Clinical applications of source localisation techniques — the human somatosensory cortex. In F. Angelieri, S. Butler, S. Giaquinto, and J. Majkowski, editors, *Analysis of the Electrical Activity of the Brain*, pp. 271–308. Wiley & Sons, Chichester, 1997.
84. W. Lutzenberger, T. Elbert, B. Rockstroh, and N. Birbaumer. *Das EEG*. Springer, Berlin, 1985.
85. N. Birbaumer and R. F. Schmidt. *Biologische Psychologie*. Springer, Berlin, 1996.
86. S. Zschocke. *Klinische Elektroenzephalographie*. Springer, Berlin, 1995.
87. A. Wunderlin. On the slaving principle. In R. Graham and A. Wunderlin, editors, *Lasers and Synergetics*, pp. 140–147, Springer, Berlin, 1987.
88. J. Dudel, R. Menzel, and R. F. Schmidt, editors. *Neurowissenschaft. Vom Molekül zur Kognition*. Springer, Berlin, 1996.
89. W. R. Adey. Molecular aspects of cell membranes as substrates for interaction with electromagnetic fields. In E. Başar, H. Flohr, H. Haken, and A. J. Mandell, editors, *Synergetics of the Brain*, pp. 201–211, Springer, Berlin, 1983.
90. E. Bracci, M. Vreugdenhil, S. P. Hack, and J. G. R. Jefferys. On the synchronizing mechanism of tetanically induced hippocampal oscillations. *J. Neurosci.*, 19(18): 8104–8113, 1999.
91. J. G. R. Jefferys. Nonsynaptic modulation of neuronal activity in the brain: Electric currents and extracellular ions. *Physiol. Rev.*, 75: 689–723, 1995.
92. K. A. Richardson, S. J. Schiff, and B. J. Gluckman. Electric field control of seizure propagation: From theory to experiment. In S. Boccaletti, B. Gluckman, J. Kurths, L. M. Pecora, R. Meucci, and O. Yordanov, editors, *Proceeding of the 8th Experimental Chaos Conference 2004*, pp. 185–196, American Institute of Physics, Melville (NY), 2004.
93. K. A. Richardson, S. J. Schiff, and B. J. Gluckman. Control of traveling waves in the mammalian cortex. *Phys. Rev. Lett.*, 94: 028103, 2005.
94. V. Braitenberg and A. Schüz. *Cortex: Statistics and Geometry of Neuronal Connectivity*. Springer, Berlin, 1998.
95. P. beim Graben and H. Atmanspacher. Complementarity in classical dynamical systems. *Found. Phys.*, 36(2): 291–306, 2006.
96. D. Lind and B. Marcus. *An Introduction to Symbolic Dynamics and Coding*. Cambridge University Press, Cambridge (UK), 1995.
97. P. beim Graben, J. D. Saddy, M. Schlesewsky, and J. Kurths. Symbolic dynamics of event–related brain potentials. *Phys. Rev. E.*, 62(4): 5518–5541, 2000.

98. P. beim Graben and J. Kurths. Detecting subthreshold events in noisy data by symbolic dynamics. *Phys. Rev. Let.*, 90(10): 100602, 2003.
99. H. Atmanspacher and P. beim Graben. Contextual emergence of mental states from neurodynamics. *Chaos and Complexity Letters*, 2(2/3), 151–168, 2007.
100. H. Atmanspacher. Contextual emergence from physics to cognitive neuroscience. *J. of Consciousness Stud.*, 14(1–2): 18–36, 2007.
101. T. Metzinger, editor. *Neural Correlates of Consciousness*. MIT Press, Cambridge (MA), 2000.
102. D. J. Chalmers. What is a neural correlate of consciousness? In Metzinger [101], Chap. 2, pp. 17–39, 2000.
103. P. beim Graben. Incompatible implementations of physical symbol systems. *Mind and Matter*, 2(2): 29–51, 2004.
104. R. Dale and M. J. Spivey. From apples and oranges to symbolic dynamics: A framework for conciliating notions of cognitive representation. *J. Exp. & Theor. Artific. Intell.*, 17(4): 317–342, 2005.